2013

Discriminating Environmental Conditions for Significant Warm Sector and Boundary Tornadoes in Parts of the Great Plains

Joshua M. Boustead
NOAA/NWS WFO Omaha/Valley

Barbara E. Mayes
NOAA/NWS WFO Omaha/Valley

William Gargan
NOAA/NWS WFO Topeka

Jared L. Leighton
NOAA/NWS WFO Topeka

George Phillips
NOAA/NWS WFO Topeka

See next page for additional authors

Authors
Joshua M. Boustead, Barbara E. Mayes, William Gargan, Jared L. Leighton, George Phillips, and Philip N. Schumacher

Discriminating Environmental Conditions for Significant Warm Sector and Boundary Tornadoes in Parts of the Great Plains

JOSHUA M. BOUSTEAD AND BARBARA E. MAYES

NOAA/NWS WFO Omaha/Valley, Valley, Nebraska

WILLIAM GARGAN, JARED L. LEIGHTON, AND GEORGE PHILLIPS

NOAA/NWS WFO Topeka, Topeka, Kansas

PHILIP N. SCHUMACHER

NOAA/NWS WFO Sioux Falls, Sioux Falls, South Dakota

(Manuscript received 20 July 2012, in final form 31 July 2013)

ABSTRACT

Using system-relative composites, based on a dataset of significant tornadoes and null supercell events, environmental conditions associated with occurrences of significant tornadoes near discernible surface boundaries were compared to nontornadic boundary supercells, and warm sector significant tornadoes to nontornadic warm sector supercells, for a portion of the Great Plains. Results indicated that significant boundary tornadoes were associated with the exit region of a 300-hPa jet maximum, while null boundary events were in closer proximity to the 300-hPa jet entrance region. The differences at 300 hPa led to significant differences at the surface, as the null composite indicated deformation and confluence into the surface boundary and enhanced frontogenesis, while this was not present in the boundary significant tornado composite. Significant synoptic differences also were noted between the warm sector tornadoes and the warm sector null events. The warm sector significant tornadoes were associated with a much stronger, negatively tilted synoptic storm system, with the composite tornado in the 300-hPa jet exit region and downstream of increasing values of absolute vorticity. Additional thermodynamic and kinematic parameters pertaining to low-level moisture and environmental winds appeared to be important in distinguishing boundary and warm sector significant tornadoes from nontornadic supercell events. Statistical comparisons between boundary and warm sector significant tornado events showed significant differences in the climatology of their length, width, and date and time of occurrence.

1. Introduction

Operational experience, numerical modeling (Atkins et al. 1999), and field experiments (Markowski et al. 1998, hereafter M98; Rasmussen et al. 2000) have shown that many significant tornadoes [Hales (1988); rated as category 2 on the Fujita scale (F2) or category 2 on the enhanced Fujita scale (EF2) or greater] occur either near a surface boundary, discernible with the current observing capabilities, or in the free warm sector of an extratropical low pressure system. Garner (2012) used a dataset of Rapid Update Cycle (RUC) analysis soundings to compare the thermodynamic and kinematic environments of boundary and warm sector significant tornadoes. In a similar fashion, this study examines a dataset of significant tornadoes from an area of the central and northern Great Plains for the period 1979–2011, using the North American Regional Reanalysis (NARR; Messinger et al. 2006). Similarities and differences in environments of boundary and warm sector significant tornadoes are compared to boundary and warm sector nontornadic supercells in the study area from 2005 through 2011 (Fig. 1).

Much of the early tornado research concentrated on patterns favorable for producing tornadoes. This pattern recognition approach gave forecasters the ability to identify situations that have been shown in the past to produce a particular phenomenon. Mook (1954)

Corresponding author address: Joshua M. Boustead, National Weather Service, 6707 N. 288th St., Valley, NE 68064.
E-mail: josh.boustead@noaa.gov

DOI: 10.1175/WAF-D-12-00102.1

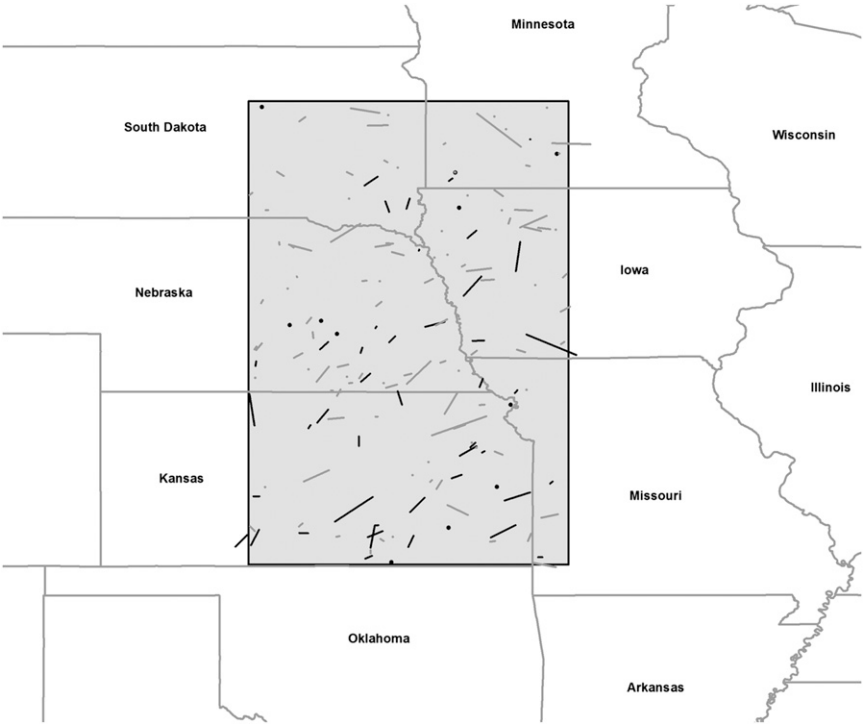

FIG. 1. Significant tornado tracks from 1979 through 2011 included in the study. The 105 boundary tornado tracks are in light gray, and the 57 warm sector tracks are in black. Thick gray lines are state boundaries.

correlated preferred thickness values for different areas of the United States to multiple tornado occurrences. Using the position of the surface low in conjunction with a cold axis at 200 hPa, Whiting and Bailey (1957) describe a method to produce a preliminary tornado forecast. Miller (1972, hereafter M72) identified five different synoptic patterns that are likely to be associated with tornadoes. In addition to identifying favorable patterns, M72 also developed a composite checklist forecasters could use operationally to recognize the occurrence of these patterns. The checklist included elements such as moisture, stability, forcing for ascent, jet streaks, and a source of dry air aloft. The M72 checklist gave values that were classified as weak, moderate, or strong. Not always directly related to tornado forecasting, the presence of an upper-level jet has been long associated with a pattern favorable for the development of severe weather (Beebe and Bates 1955; McNulty 1978; Uccellini and Johnson 1979; Rose et al. 2004; Clark et al. 2009). Much of the early pattern recognition tornado research identified a strong synoptic-scale system, including an upper-level jet maximum, differential cyclonic vorticity advection, and surface fronts. Maddox and Doswell (1982) noted that not all intense severe weather events are associated with a strong synoptic-scale weather system. They examined the role of strong low-level warm air advection (WAA) in producing severe convection when large-scale vorticity patterns were weak.

The identification of synoptic patterns favorable for severe weather and tornadoes also has been completed for specific geographical areas. Lowe and McKay (1962) developed composite charts at 850, 700, 500, and 200 hPa associated with tornadoes in the Canadian prairies. Doswell (1980) showed the evolution of the synoptic pattern associated with severe weather occurrences over the high plains of the United States. Hagemeyer (1997) identified common characteristics associated with Florida tornado outbreaks. Monteverdi et al. (2003) provided shear values associated with central and northern California tornado events. Gaffin and Parker (2006) completed composite charts and a climatology of significant tornadoes across the southern Appalachian region. Research has also examined severe weather development in differing geographical areas within one particular flow pattern. Johns (1984) examined severe weather events that are associated with upper-level flow from the northwest. Johns indicated these events typically occur in the late spring and summer. He noted the presence of strong low-level WAA near the onset of the event, as well as the importance of directional wind shear in the

vertical, especially later in the season when speed shear is reduced due to weakening tropospheric flow.

As knowledge of the environments that produce significant tornadoes increased, along with increased documentation of significant tornado events and the development of gridded datasets, climatologies of meteorological parameters were developed to provide operational forecasters with a range of values to help anticipate their occurrence. Rasmussen and Blanchard (1998, hereafter RB98) examined several parameters related to thunderstorms and found that the threat of supercells improved with increasing shear. They found that good discriminators for significant tornadoes were the energy–helicity index (EHI; Hart and Korotky 1991) and the vorticity generation parameter (VGP; Rasmussen and Wilhelmson 1983), though they indicated a high false alarm ratio with these parameters. Thompson et al. (2003, hereafter T03) used RUC-2 proximity soundings to analyze the convective environment near supercells. They found the most significant differences were in the 0–1-km storm-relative helicity (SRH; Davies-Jones et al. 1990), 0–1-km relative humidity, and the 100-hPa mixed layer (ML) lifted condensation level (LCL). A similar study by Craven and Brooks (2004, hereafter CB04) using a dataset of rawinsonde soundings from 1997 to 1999 found the 0–1-km shear and MLLCL discriminated best between significant tornadoes and other severe convection. Davies (2004) showed that the use of the ML convective inhibition (CIN) and the ML level of free convection (LFC) could help to discriminate between nontornadic, tornadic, and strong tornado-producing thunderstorms. Grams et al. (2012, hereafter G12) showed that convective mode also was a good discriminator between significant tornado events and other severe thunderstorms.

The presence and impact of a boundary on storm morphology also has received considerable research attention (Purdom 1976; Maddox et al. 1980; Weaver and Purdom 1995; M98; Rasmussen et al. 2000). Maddox et al. (1980) suggested that a storm that develops within a unidirectional low-level wind profile would encounter enhanced vertical vorticity as it nears and then crosses a boundary. The enhancement in vertical vorticity near a boundary is due to increased directional low-level turning to the wind profile near and on the cool side of the boundary as cold air advection (CAA) decreases the veering of the wind profile with height. During the Verifications of the Origins of Rotation in Tornadoes Experiment (VORTEX; Rasmussen et al. 1994), 70% of tornadoes rated as F1 or higher ($\geq$F1) were observed to be associated with a preexisting boundary (M98). It was shown that the area from 10 km on the warm side to 30 km on the cool side of the boundary was a favorable region for tornado development. Through numerical simulations (Atkins et al. 1999) and field studies such as VORTEX, it has been shown that boundaries may increase the low-level horizontal vorticity. A supercell interacting with this enhanced low-level vertical vorticity can lead to low-level mesocyclone formation. Although the majority of tornadoes during VORTEX were associated with a boundary, 30% occurred with no discernible preexisting boundary. Rasmussen et al. (2000) and Schumacher and Boustead (2011) indicated that tornadoes without a discernible boundary were more likely when the ambient low-level horizontal vorticity was near values observed in association with boundaries. This generally would happen when there was extreme environmental shear resulting in high values of SRH. The 3 May 1999 Oklahoma outbreak (Thompson and Edwards 2000), the 1965 Palm Sunday tornado outbreak (Koch et al. 1998), and the 3–4 April 1974 Super Outbreak (Corfidi et al. 2010) are examples of warm sector significant tornadoes without discernible surface boundaries.

Improvements in our understanding of the environments that produce tornadoes have led to advances in both our operational knowledge and model forecasts, permitting forecasters to utilize an ingredients-based approach to severe weather forecasts. These ingredients can be produced by model forecasts at longer time ranges, and can be observed using satellite, radar, and vertical wind profilers in the near term. Model forecasts can be in error, though, and observing systems are limited in both space and time, thus providing forecasters the opportunity to add potentially significant value to the forecast. The ability of forecasters to recognize when a severe weather forecast does not fit a particular pattern for a geographical area or a synoptic flow pattern allows forecasters to determine when value can be added to the forecast. This is especially true at longer ranges of the forecasts where models, including convection-allowing models (CAMs), decrease in accuracy (Weisman et al. 2008). Johns and Doswell (1992) indicated that pattern recognition and climatological studies would continue to play an important role in operational meteorology. Despite the ever-increasing computer power and forecaster knowledge of tornadoes, this is likely still true today and will be for some time into the future. By combining pattern recognition with new tools, such as CAMs and new observing systems, forecasters have the potential to be able to recognize situations that can produce significant tornadoes and distinguish those from environments that would support nontornadic supercells.

To help operational forecasters, this study uses system-relative composites similar to those in Moore et al. (2003) and Glass et al. (1995) to compare and contrast patterns of ingredients that are associated with significant

tornadoes near discernible boundaries and in the warm sector to nontornadic boundary and warm sector supercells. Thunderstorms occur on the meso-Γ scale, and forcing for their development generally occurs on the meso-α scale. Nevertheless, synoptic-scale environments can produce favorable conditions for convective initiation, and those times when both the synoptic and mesoscale environments are favorable for tornadoes are generally when the largest outbreaks occur (Doswell 1987). Doswell et al. (1993) indicated that as many as 90% of tornado events may not be synoptically evident. The patterns presented in this paper, especially in relation to the boundary-only events, may provide forecasters with pattern recognition to add value to the tornado forecast. By testing for the statistical significance for differences in synoptic-scale and mesoscale features, forecasters may use these results to better identify favorable patterns for tornadoes, especially along boundaries.

2. Methodology

Significant tornadoes for the years 1979–2011 for parts of the central and northern plains were compiled using the National Climatic Data Center (NCDC) publication *Storm Data* (Fig. 1). For each tornado occurrence, archived surface observations were obtained and plotted using the Digital Atmosphere program for a period of 2 h before to 1 h after tornadogenesis. Hand-drawn analyses of temperature, dewpoint, and pressure were completed for each of the hours. Using the manual surface analyses, boundaries were classified as the separation of two differing air masses with either a temperature or moisture discontinuity, including cold fronts where colder air was overtaking a warmer air mass, retreating warm fronts with warmer air overtaking a cooler air mass, stationary boundaries with little or no discernible movement of the differing air masses, drylines, and outflow boundaries. The cool side of the boundary refers to the side of the boundary that has lower temperatures, while the warm side has higher temperatures. No additional information sources were used to identify boundaries. Once the subjective surface analyses were completed for each occurrence, the significant tornado was plotted on the analysis. Following findings from M98, if the tornadogenesis point was located within 10 km on the warm side or up to 30 km on the cool side of the analyzed boundary, the event was classified as a boundary event. If there were no discernible surface boundaries present at the tornadogenesis point, the event was classified as a warm sector case. No additional classification of tornadoes by boundary type was made.

A number of uncertainties exist when determining if the starting point of the tornado is near a boundary, including both time and location errors in *Storm Data*. Another source of uncertainty is in the boundary placement, given the limited number of surface observations available for the analyses, particularly early in the climatology. With VORTEX, high-resolution mobile surface observations were combined with stationary and mobile radar, satellite, and aircraft data to mitigate some of these potential errors. This study uses standard surface observations available to operational forecasters, including the Automated Surface Observing System (ASOS) and Automated Weather Observing System (AWOS), resulting in a higher degree of potential uncertainty in precise boundary placement.

In several instances, more than one significant tornado occurred in a single event within the study domain, with both significant boundary and warm sector events in the same 24-h period. In these cases, only the first significant tornado during a particular 24-h period was included in the study, and preference was given to the first warm sector significant tornado when both types occurred in order to increase the sample size of the warm sector cases. Completed classification resulted in 57 warm sector and 105 boundary significant tornado event days.

Nontornadic databases were developed for comparison to both the significant boundary and warm sector tornado databases. This was accomplished by obtaining hail reports >4.45 cm (1.75 in.) from *Storm Data* for the years 2005–11. The criteria of hail > 4.45 cm was chosen to limit the number of potential cases and increase the likelihood that the remaining cases may be supercells. The hail database then was compared to a database of tornadoes from the same time period. Any days when large hail and tornadoes were observed in the study area were then removed from the database. For the remaining hail reports in the database, subjective surface analyses were completed for 2 h prior to 1 h after the initial hail report in a particular 24-h period, using the same method as with the significant tornadoes. The hail reports were then classified as boundary or warm sector events.

Archived level II Weather Surveillance Radar-1988 Doppler (WSR-88D) data for the closest radar to the significant tornado or hail reported were obtained from the NCDC Hierarchical Data Storage System (HDSS) Access System (http://hurricane.ncdc.noaa.gov/pls/plhas/has.dsselect). Radar data were obtained for 15 min prior to 5 min after tornadogenesis or the occurrence of the large hail. If the full time period was not available from the archive, the event was not used. The radar data were analyzed using Gibson Ridge GR2 Analyst software to determine if the parent thunderstorm producing the significant tornado or large hail was a supercell. For the purposes of this study, a thunderstorm was required

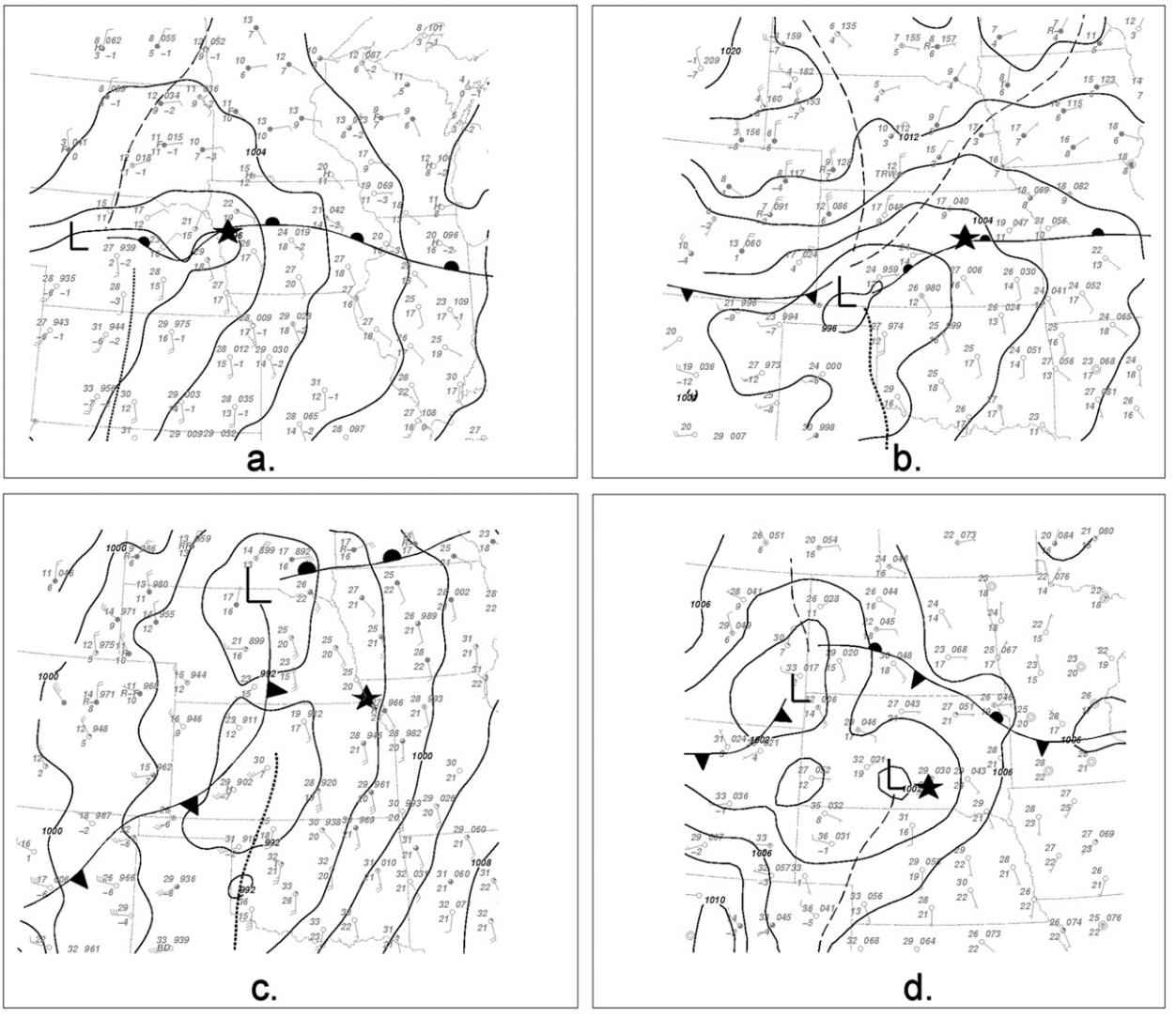

FIG. 2. Subjective surface analysis of (a) a boundary significant tornado event from 9 Apr 2011, (b) a nontornadic boundary event from 6 May 2010, (c) a warm sector significant tornado event from 5 Jun 2008, and (d) a nontornadic warm sector event from 30 Jul 2008. Solid black contours show sea level pressure contoured every 2 hPa. Fronts are standard except that surface troughs are denoted as dashed black lines and drylines are black dotted. Station plots include temperatures and dewpoints (°C) and sea level pressure (hPa). Winds are in meters per second (half barb is equal to 2.5 m s^{-1} and a full barb is 5 m s^{-1}). The solid star in all plots is the location of (a),(c) tornadogenesis or (b),(d) large hail reports.

to maintain $\geq$10 m s^{-1} of rotational velocity across a distance of $<$10 km on two adjacent elevation angles for at least three consecutive volume scans to be classified as a supercell, similar to the criteria in Bunkers et al. (2006). Events with improperly dealiased radar data were not used. Using this method, it was determined for 105 (57) significant boundary (warm sector) tornado cases that 95% (90%) were associated with supercells. For null cases, only supercells were used, and this technique resulted in 41 (20) individual supercell boundary (warm sector) events. Example surface analyses from each dataset are presented in Fig. 2.

For each event, NARR data were obtained from the NCDC National Operational Model Archive and Distribution System (NOMADS) website (http://nomads.ncdc.noaa.gov). The NARR includes 45 vertical levels and 32-km grid spacing and does allow for analyzing the general convective environment (Gensini and Ashley 2011). The NARR was preferred because it provided a long-term, relatively high-resolution model over North America, allowing for a larger significant tornado database, and because of the consistency of the model, with verification indicating significant improvement in accuracy over the National Centers for Environmental

Prediction–Department of Energy Global Reanalysis (Messinger et al. 2006). Analysis of the NARR mesoscale convective environment indicated some discrepancies from previous significant tornado research, especially for parameters that included wind fields near and below 1 km. To make the study results more operationally relevant to forecasters and comparable to past research, archived Storm Prediction Center (SPC) surface objective analyses (SFCOAs; Bothwell et al. 2002) were obtained and analyzed for events from 2005 through 2011. The SPC SFCOA approach uses objectively analyzed surface observations as a first-guess field, along with the Rapid Update Cycle-2 (RUC-2; Benjamin et al. 1998), to create a three-dimensional objectively analyzed analysis grid. For the purposes of this study, analyses of specific values of NARR thermodynamic and kinematic convective parameters were done only to provide a statistical comparison between the boundary and warm sector significant tornado events to the nontornadic databases. Although the NARR quantities themselves presented here may have limited operational utility, the comparisons of the means of the values do have operational utility, as all four categories of cases being compared used a consistent database to create those comparisons. The NARR was supplemented with RUC to provide a scale for use in operations.

NARR data are available every 3 h, and the first available model run preceding tornado or hail development was used in this study. The NARR data were displayed using the General Meteorological Package (GEMPAK; desJardins et al. 1991), and system-relative composites were created using each event from the warm sector and boundary significant tornadoes, as well as warm sector and boundary null events. The composites were developed centered on the touchdown location of the significant tornado and the location of the large hail. The RUC is created hourly, and the first available analysis prior to the significant tornado or null event was obtained.

To assess whether differences in the distribution of convective elements, such as temperature, moisture, and wind, were significant, the Wilcoxon–Mann–Whitney (WMW; Wilks 1995) test was used, similar to the approach in Coniglio et al. (2010). The WMW is a nonparametric statistical test that allows for the analysis of two different datasets to determine the confidence in the differences. The WMW test was completed at each grid point in the dataset and is displayed in a two-dimensional plan view, allowing for visualization of where in the domain the two datasets are statistically different. To assess the location of the significant tornado in relation to the sea level pressure pattern for both boundary and warm sector events, the NARR data were used to create a surface low relative tornado analysis. This was accomplished by using the location of the tornado in relation to the lowest sea level pressure east of the Rocky Mountains and west of 88°W. Finally, using the NARR data from the location of the tornadoes and hail, various thermodynamic and kinematic convective parameters were analyzed in the national version of the Skew-*T* Hodograph Analysis and Research Program (NSHARP; Hart and Korotky 1991). Additional statistical analyses determined the significance of differences in the means and variances of a number of parameters between the boundary and warm sector tornado populations. With population sizes of $n = 105$ and 57, respectively, a Student's t test was adequate to compare the means of the two samples (Dowdy et al. 2004). The differences in variances between the boundary and warm sector populations for the same parameters also were examined using an F test. In both cases, significance was noted at a threshold of at least 95% confidence and above ($\alpha = 0.05$).

3. Results

a. Climatology of the events

The pathlength, maximum width, time of occurrence, and day of year, as documented in *Storm Data*, were compared between the warm sector and boundary tornado samples to determine differences in both the means and the variances of the samples (Table 1). Using a Student's t test with $\alpha = 0.05$, the mean pathlength of warm sector cases [20.60 km (12.80 mi)] was determined to be significantly longer than that of boundary tornadoes [13.28 km (8.25 mi)]. Additionally, using an F test with $\alpha = 0.05$, the variance of the two samples also was significantly different, with warm sector tornadoes exhibiting significantly greater variance than boundary cases. The findings for pathlength were internally consistent, as one would expect that the increased range of pathlengths in the warm sector cases would include longer paths that would contribute to a greater mean pathlength, as well. The mean maximum widths were not significantly different between warm sector and boundary cases, but once again, the variance of the warm sector tornado widths was significantly greater than the boundary tornado widths.

Most significant tornadoes in the study occurred during the late afternoon or early evening and in the late spring to early summer months (Table 2). Though events between midnight and noon were rare in both samples, boundary-only events included more morning events, while all but two warm sector events all occurred from 1400 (2000) through 2400 (0600) local standard time (UTC). More warm sector than boundary events occurred during the nonpeak months of November–February. The results were confirmed by statistical analysis, as the variance of the time of occurrence of boundary tornadoes

TABLE 1. Mean and variance results for boundary and warm sector significant tornadoes for length, width, time, and date. Boldface numbers show statistically significantly greater means and variances.

Category	Length (km)	Width (m)	Time (CST)	Date (Julian)
Boundary (mean)	13.28	316.50	1704	166.49
Variance	170.64	164298.9	**1221**	2098.75
Warm sector (mean)	**20.60**	405.43	1735	154.02
Variance	**269.78**	**388782.8**	0706	**3796.60**

was significantly greater than that of warm sector tornadoes, though the mean times of occurrence were not significantly different. The variance of the date of occurrence of warm sector tornadoes was significantly greater than that of boundary events, though again, the means were not significantly different.

b. Synoptic environment

The system-relative synoptic-scale composite patterns were compared for boundary significant tornado events and nontornadic boundary events, as well as for warm sector significant tornado events and nontornadic warm sector events. In both boundary composites, southwest flow was indicated at 300 hPa, with a trough indicated upstream from the report location and a ridge downstream (Figs. 3a and 3b). Southwest flow was observed in 59% (67%) of the tornadic (nontornadic) events. A 300-hPa jet maximum was located downstream from the report location in both the boundary tornado and null boundary composites, but in the null boundary composite, this jet was located much closer to the report location. The downstream ridge axis also was less amplified in the null boundary composite than in the boundary tornado composite, with the upstream trough positively tilted. In the boundary tornado composite, a jet maximum was located upstream of the tornado report, and both composites indicate an area of divergence at 300 hPa near the report location. Clark et al. (2009) showed the vertical velocity and associated ageostrophic circulation vectors for storm reports in the entrance and exit regions of jets streaks. They indicated a pronounced

TABLE 2. Number of events in relation to time of year and day for boundary events and warm sector events. Numbers in parentheses are the null events. Numbers are boldface where there are three or more events indicated for that hour. Time is in CST.

Boundary events

	0	1	2	3	4	5	6	7	8	9	10	11	12	13	14	15	16	17	18	19	20	21	22	23	Totals
Jan																									
Feb																									
Mar																**3**		1	(1)						4 (1)
Apr													(1)	(2)		1 (1)	1 (2)	2	**4**	1	2			1	12 (6)
May									1					1	1	2 (1)	**4**	**5**	1 (1)	**4 (1)**	(1)			1	20 (4)
Jun		1		1							1		(1)	3	**3 (1)**	**3**	**4 (1)**	2 (1)	**7 (1)**	**6 (1)**	**3 (1)**	2		1	37 (7)
Jul						1			1						**3**	1	2 (2)	1 (1)	**3**	2 (1)	(2)				14 (6)
Aug												(1)		(2)			(2)	**4 (1)**	**1 (4)**	**3 (1)**	1 (1)	1	2		12 (12)
Sep																	(2)	1	(1)	2	1	(1)			4 (4)
Oct																	(1)	1	1						2 (1)
Nov																									
Dec																									
Totals		1		1		1			2			1 (1)	(2)	4 (4)	7 (1)	10 (7)	17 (7)	13 (7)	20 (4)	15 (4)	6 (5)	4		3	

Warm sector events

	0	1	2	3	4	5	6	7	8	9	10	11	12	13	14	15	16	17	18	19	20	21	22	23	Totals
Jan																		1							1
Feb																				1					1
Mar																	2		1 (1)	1					4 (1)
Apr										1						1	1	2 (1)	2	2 (1)		1		1	11 (2)
May	1											1			2 (2)	**4**	**6**	2	2	**3 (1)**	2	1	1		25 (3)
Jun														(1)		1	1	**1 (3)**	2	2 (2)	**3**				10 (6)
Jul															(1)	(1)		(1)	(2)	1 (1)					1 (6)
Aug																	2			1				1	4
Sep																2		1		1					4
Oct															1 (1)	1	1			1					4 (1)
Nov															1			(1)							1 (1)
Dec																									
Totals	1									1		1		(1)	4 (4)	9 (1)	13	7 (5)	7 (3)	13 (5)	5	2	1	2	

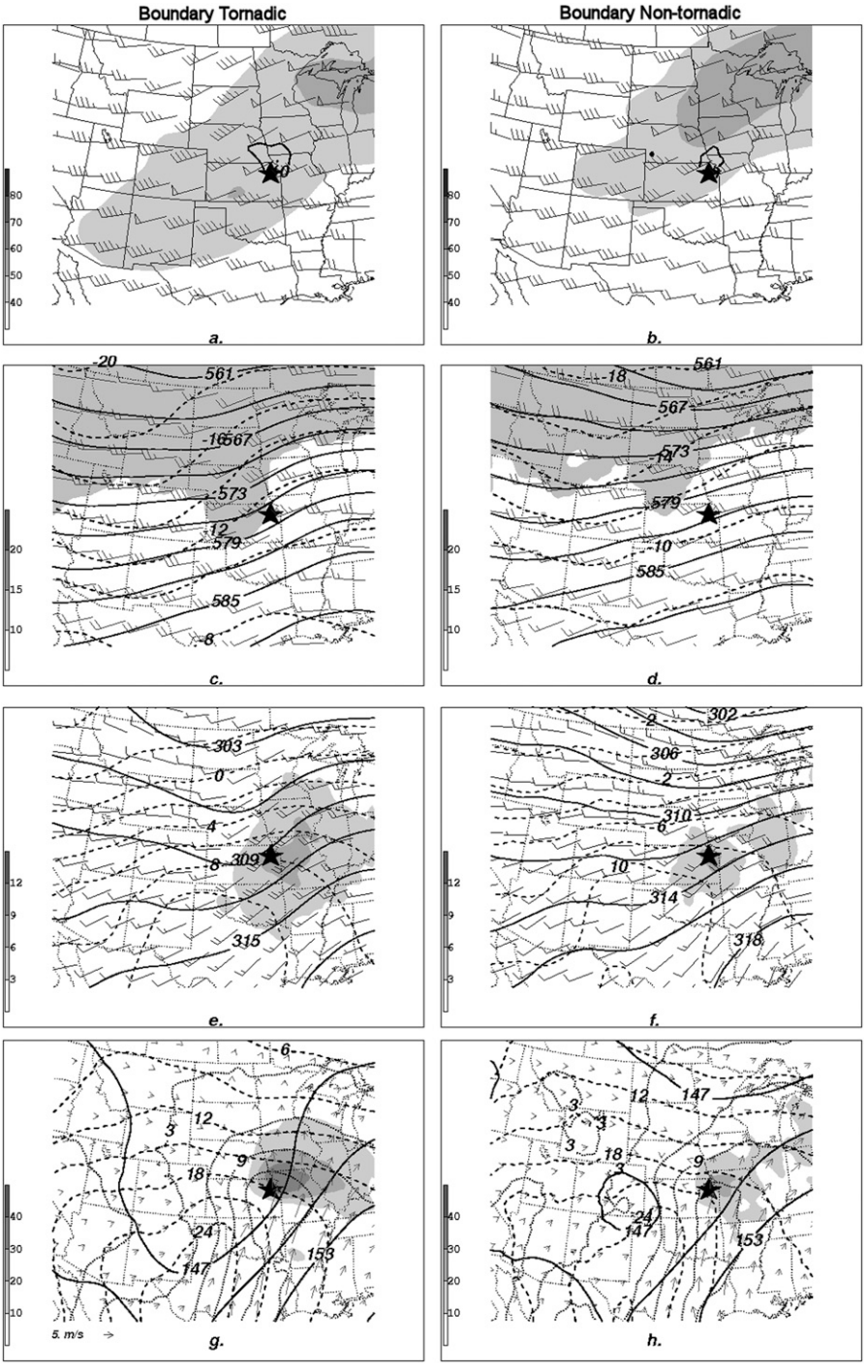

FIG. 3. Boundary system-relative composites of mandatory pressure levels, with (left) boundary tornado and (right) null boundary events. Map background is for scale reference only. (a),(b) Contours at 300 hPa are divergence (10^{-5} s $^{-1}$), wind isotachs are shaded every 20 m s^{-1}, and wind barbs are in kt (kt = 0.51 m s^{-1}, half barb is equal to 2.5 m s^{-1}, a full barb is 5 m s^{-1}, and a flag is 25 m s^{-1}). (c),(d) Height lines at 500 hPa are contoured in solid black every 30 m, dashed black contours are temperature every 2°C, and absolute vorticity is shaded (1×10^{-5} s^{-1}). (e),(f) At 700 hPa, the heights are contoured in solid back every 30 m, temperature is shown by dashed lines contoured ever 2°C, and positive temperature advection is shaded > 3 K (12 h)$^{-1}$. (g),(h) At 850 hPa, the heights are contoured in solid black lines every 30 m, dashed black contours are temperature every 2°C, dotted black contours are dewpoint temperature every 2°C, positive θ_e advection is shaded (10^{-1} K h^{-1}), and moisture transport is shown by vectors [g m (kg s)$^{-1}$]. The solid star represents the system-relative tornado or null event in all panels.

response of northern ageostrophic flow into the jet axis for reports in the entrance region, while the exit region showed deep ageostrophic southerly flow on both sides of the jet axis.

Both boundary composites indicated a low-amplitude short-wave trough with increasing values of absolute vorticity 300–400 km upstream from the report location at 500 hPa (Figs. 3c and 3d). The short-wave trough in the boundary tornado composite had a neutral to negative tilt, with the composite tornado located near the 500-hPa no-change temperature line. The null boundary composite depicted a trough with a positive tilt and weak WAA occurring at the report location. A smoothed 500–300-hPa **Q**-vector analysis indicated forcing for large-scale ascent near the location of the significant tornado, while the null boundary composite indicated the report position was located near the southern edge of this forcing for ascent (not shown). The speed and direction of the boundary tornadic 500-hPa winds were closer to the values G12 found for northern plains summer tornadoes.

The boundary 700-hPa composites reveal WAA near the location of the report that was stronger and more expansive in the boundary tornado composite than in the null boundary composite (Figs. 3e and 3f). Consistent with 300 and 500 hPa, the short-wave trough associated with the boundary tornado composite had a neutral tilt compared to the more positive tilt of the null boundary composite. The 700-hPa temperatures for the boundary significant tornado composite were cooler than those indicated for the null composite. These results were consistent with Bunkers et al. (2010), who found that for the Great Plains, 700-hPa temperatures associated with significant tornadoes were cooler than those associated with significant hail. The 700-hPa temperatures found at the tornadogenesis location also were consistent with values found by G12 and associated with northern plains summertime tornadoes.

The 850-hPa boundary composites have several similarities, including the event location near the northern edge of the moisture axis, on the northwestern edge of the strongest moisture transport vectors, northeast of the 850-hPa temperature axis, and east of the lowest heights (Figs. 3g and 3h). The 850-hPa dewpoint temperatures in both boundary composites near the event location were similar to those indicated by G12 for southern plains spring tornadoes. The most significant difference in the 850-hPa composites was related to θ_e advection. The boundary tornado composite indicated statistically significantly stronger θ_e advection near and to the north and east of the report location than the null boundary composite (Fig. 4). This pattern was consistent for levels below 850 hPa as well (not shown). At 850 hPa, stronger wind speeds were apparent in the boundary tornado events compared to the null boundary cases (not shown). For the boundary tornado cases, 59% had wind speeds $>10\,\mathrm{m\,s^{-1}}$ compared to 21% of the null boundary cases. The boundary tornado wind speeds were similar to the 850-hPa wind speeds for northern plains summer tornadoes found by G12 (not shown).

Differences between the boundary tornado and null boundary composites were reflected at the surface, as well, that appear to support the entrance and exit jet circulations shown by Clark et al. (2009). In both system-relative boundary composites, a surface low pressure system was located over northwest Kansas with a warm front extending east to near the location of either the significant tornado or the null event. In Fig. 5, significant differences exist in surface deformation along the warm front. In the null boundary composite, the surface streamlines along and north of the warm front exhibit confluence, while in the boundary tornado composite, little surface confluence in the wind field was found near tornadogenesis, with more confluence indicated to the north of the low pressure along an inverted trough. The orientation of the axis of dilatation to the isentropes resulted in frontogenesis and potential strengthening of the temperature gradient that is not observed in the tornado composite. The increased temperature gradient and associated change in the surface wind field may limit the tornado potential in the null boundary composite, due to increased static stability (see Fig. 12 and section 3d for further analysis). Although there is the potential that an increase in the temperature gradient may lead to increased vorticity and stronger lift along the surface boundary, as Maddox et al. (1980) pointed out, tornado potential may actually decrease as storms move across the boundary deeper into the cold air.

Past studies have pointed out the importance of low-level moisture in the development of tornadoes (M72, RB98, G12). Limited low-level moisture can lead to higher LCL heights and an increased risk for the outflow associated with supercells to become dominant and decrease the tornado threat. The mean surface dewpoint temperature for the boundary tornadogenesis location was 19°C, which is the same mean value found by G12. While the surface dewpoint for the null boundary cases was lower (17°C), it appears in this study that the most significant difference was the surface dewpoint depression. Statistically significantly lower dewpoint depressions were noted in the boundary tornado composite compared to the null boundary composite (Fig. 6), with a mean value of 8.5°C at the boundary tornadogenesis location and 13.8°C at the null boundary event location.

The comparison of system-relative synoptic-scale composites for warm sector events produced more noticeable differences than the boundary composites. At 300 hPa,

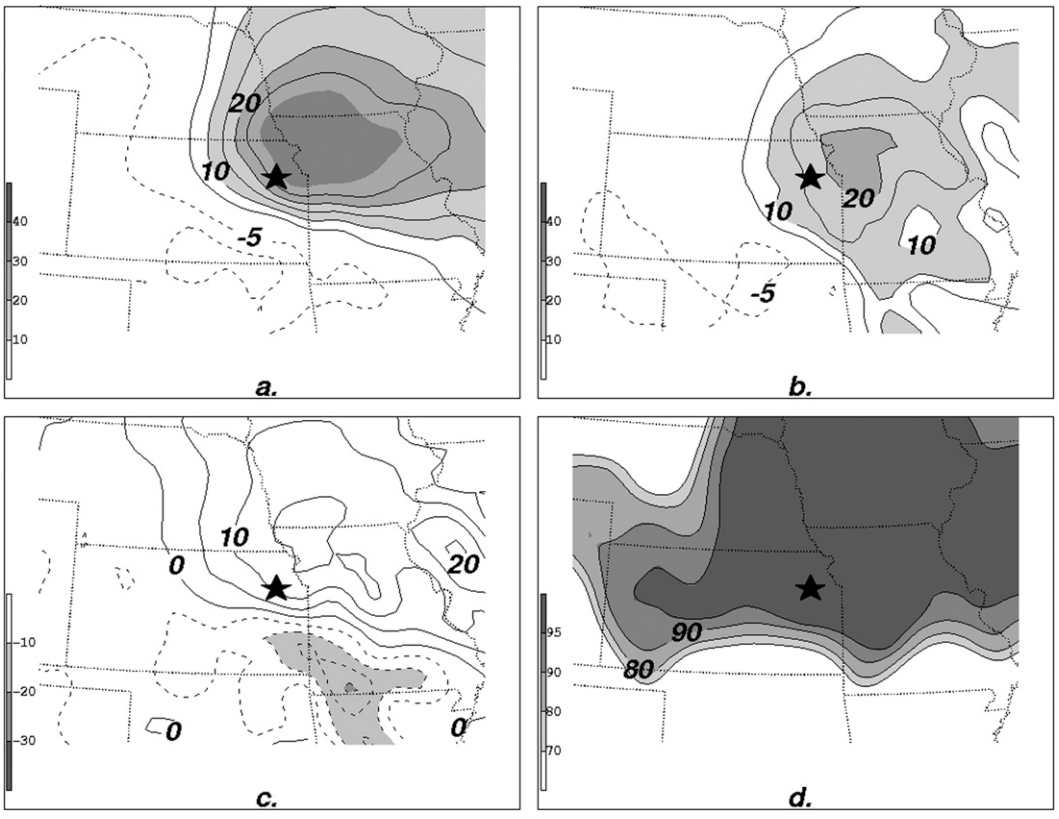

FIG. 4. Boundary system-relative composite of 850-hPa θ_e advection (10^{-1} K h^{-1}) with positive (negative) values in solid (dashed) black lines contoured every 5×10^{-1} K h^{-1} (shaded every 10×10^{-1} K h^{-1} for positive values) for (a) tornado and (b) null events. (c) The difference for tornado minus null events, shaded when null values are greater. (d) The results of the WMW significance test shaded for confidence >70%.

there was a significantly stronger jet maximum in the warm sector tornado composite than in the null warm sector composite (Figs. 7a and 7b). Of the warm sector tornado events, 67% were associated with wind speeds > 31 m s^{-1} compared to 25% of the nontornadic events at the grid point nearest tornadogenesis or large hail. Southwest flow was indicated in 91% of the warm sector tornado composite events, with the tornadogenesis location in the exit region of the jet maximum and an area of horizontal divergence near and to the north and east. In the null warm sector composite, the flow was generally zonal, with 60% having a wind direction $> 270°$ with a jet streak located approximately 1100 km upstream. There was also an apparent downstream jet located approximately 1000 km northeast of the report location.

The warm sector 500-hPa significant tornado composite (Fig. 7c) resembles the type 2 M72 tornado-producing pattern, with a high-amplitude, progressive, negatively tilted upper-level trough associated with strong height falls, and with increasing values of absolute vorticity upstream of the tornadogenesis location. Similar to the boundary tornado composite, the warm sector tornado composite indicated forcing for large-scale ascent in the 500–300-hPa **Q**-vector analysis at the location of tornadogenesis (not shown). The 500-hPa null warm sector composite (Fig. 7d) showed a low-amplitude short-wave trough associated with increasing values of absolute vorticity upstream of the report location, but the trough was weaker with weaker large-scale forcing for ascent. The warm sector tornado events had wind speeds similar to those shown by G12 for southern plains spring tornadoes, while both 500-hPa warm sector composites had temperatures similar to G12 for spring southern plains tornadoes.

In the 700-hPa warm sector tornado composite, a negatively tilted trough was evident that was deeper than the null warm sector composite, with the tornado located approximately 300 km downstream from the trough axis (Fig. 7e). The null warm sector 700-hPa composite indicated a positively tilted trough, with the report location approximately 450 km to the southeast of the trough axis (Fig. 7f). The 700-hPa temperatures for the significant tornado composite were similar to findings from Bunkers et al. (2010) and also were consistent for spring southern

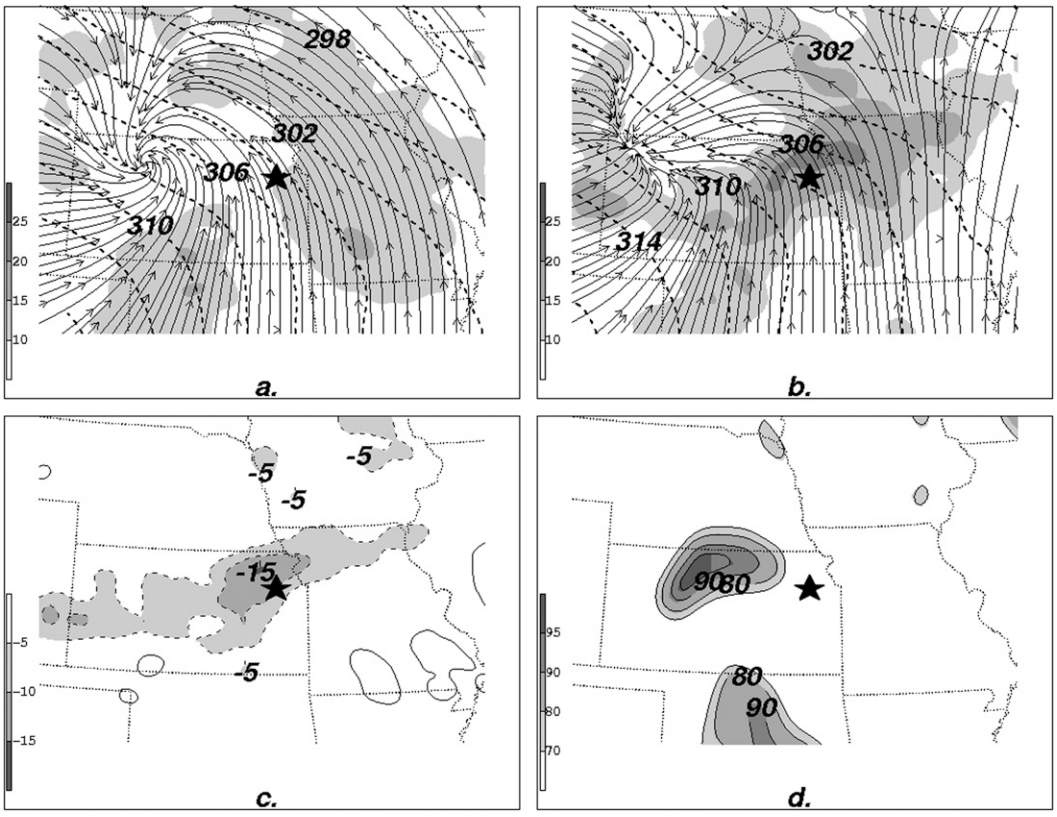

FIG. 5. As in Fig. 4, but for 10-m deformation, shaded for values $>10\ s^{-5}$. Dashed contours are potential temperature contoured every 2 K. Streamlines are 10-m winds.

plains tornadoes described by G12. The orientation of the trough at 700 hPa led to statistically significant differences in the temperature advection, as the warm sector tornado composite tornadogenesis location was near the no-change temperature line with WAA occurring downstream, while the null warm sector composite indicated broad WAA occurring near the report location (Fig. 8).

Tornadogenesis in the 850-hPa warm sector tornado composite occurred to the southeast of the lowest heights, while the null warm sector composite had the report location to the southeast of a positively tilted trough (Figs. 7g and 7h). In both 850-hPa composites, the event location was within the moisture axis and near the western edge of the strongest moisture transport vectors, but the tornado composite had higher dewpoint temperatures similar to those shown by G12 for southern plains tornadoes. For both warm sector composites, the reports were to the east of the axis of the highest 850-hPa temperatures. In both of the 850-hPa warm sector composites, the strongest θ_e advection was located to the north and east. The wind direction and speed for the 850-hPa warm sector tornadoes were similar to those found by G12 for southern plains tornadoes, with 38% having wind speeds $>15\ m\ s^{-1}$ and 50% with a wind direction between 169° and 191° (not shown).

As with the boundary composites, low-level moisture was a significant factor for the warm sector composites. The mean values of surface dewpoint temperatures for the warm sector tornado composites were less than those in the boundary composites, with 17°C (16°C) for the warm sector tornado (null) composites. Despite the lower dewpoint temperatures in the warm sector composites, cooler warm sector surface temperatures allowed for similar dewpoint depressions to those seen in both the boundary tornado and warm sector tornado composites (Fig. 9). The significantly lower dewpoint depressions near and downstream of the tornado, compared to the null warm sector events, likely contributed to lower LCL heights and an increased tornado risk.

Some seasonal variance to the significant tornadoes for both boundary and warm sector cases is visible when the tornadoes are plotted relative to the area of low surface pressure. Overall, boundary events tended to occur to the east and northeast of the area of lowest surface pressure (Fig. 10a). From a seasonal perspective, the majority of

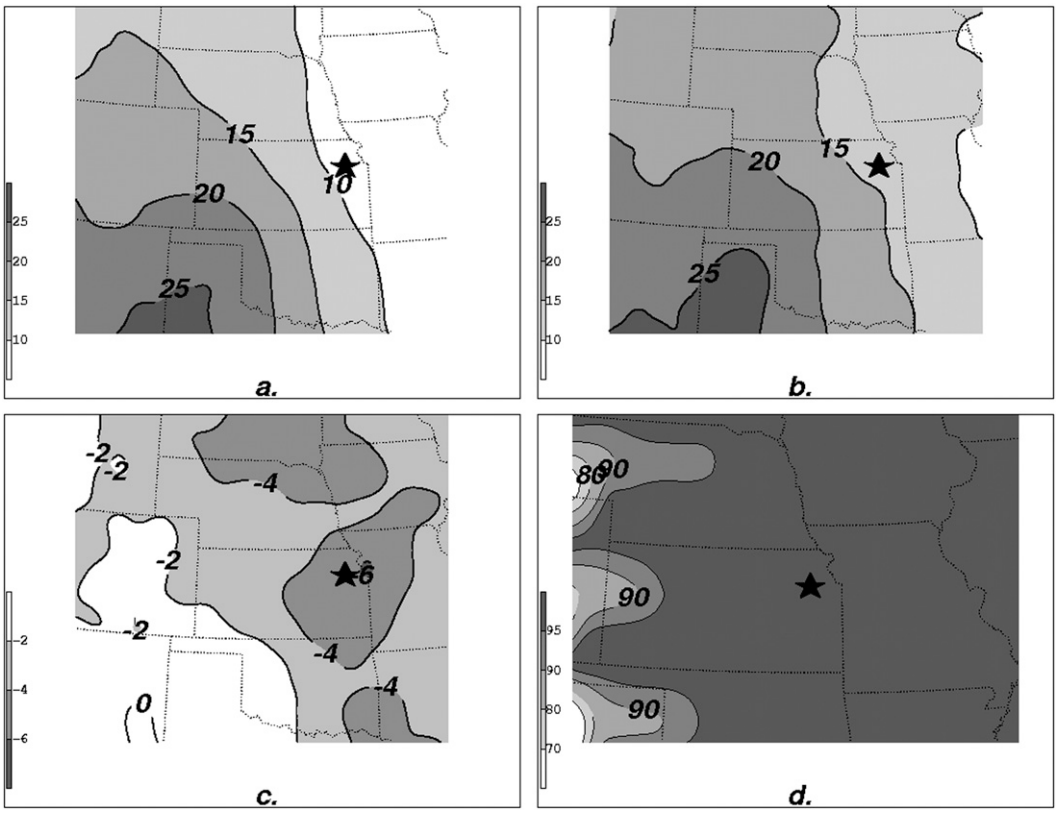

FIG. 6. As in Fig. 4, but for 2-m dewpoint depression (°C), shaded every 5°C for values >10°C.

the May and June boundary events were located along and north of the latitude of the lowest pressure. It was notable that the majority of the events that occurred to the south of the latitude of lowest surface pressure were July and August events. Although limited in numbers, all September–November tornadoes occurred to the northeast of the area of lowest pressure. In general, the warm sector significant tornadoes occurred from the south through east of the area of lowest pressure (Fig. 10b). The majority of the January–April warm sector events occurred along and south of latitude of the area of lowest pressure. May and June warm sector events tended to occur in two different areas, one just ahead and northeast of the area of lowest surface pressure, and another cluster >400 km to the south, possibly delineating two distinct patterns favorable for spring warm sector significant tornadoes in this part of the Great Plains. Few July and August warm sector significant tornadoes were reported, but in general, they occurred to the south of the area of lowest pressure.

c. *Convective environment*

The NARR data for each tornadogenesis and null report location in the dataset were analyzed using the program NSHARP (Hart and Korotky 1991). This allowed for a statistical analysis and box-and-whiskers plots for various thermodynamic and kinematic parameters to be calculated. Statistically significant differences were noted in ML convective available potential energy (CAPE), MLLCL, and MLLFC (Fig. 11). Although the Student's t test for MLCAPE indicated that the means of the boundary and warm sector tornado events were significantly higher than the means for their respective null cases, the overlap in the inner quartiles indicated this might have somewhat limited use operationally to distinguish boundary (warm sector) significant tornado events from the nontornadic boundary (warm sector) events (Fig. 11a). The subsynoptic pattern of lowest 180-hPa most unstable (MU) CAPE and CIN does illustrate the differences in favored location for significant tornadoes (Fig. 12). The composite location of the boundary significant tornado is near the apex of the higher MUCAPE and in a region of lower MUCIN compared to lower values of MUCAPE and higher MUCIN in the nontornadic boundary composite (Figs. 12a and 12b). In the warm sector, the MUCAPE axis is oriented north to south, in most cases ahead of a dryline or

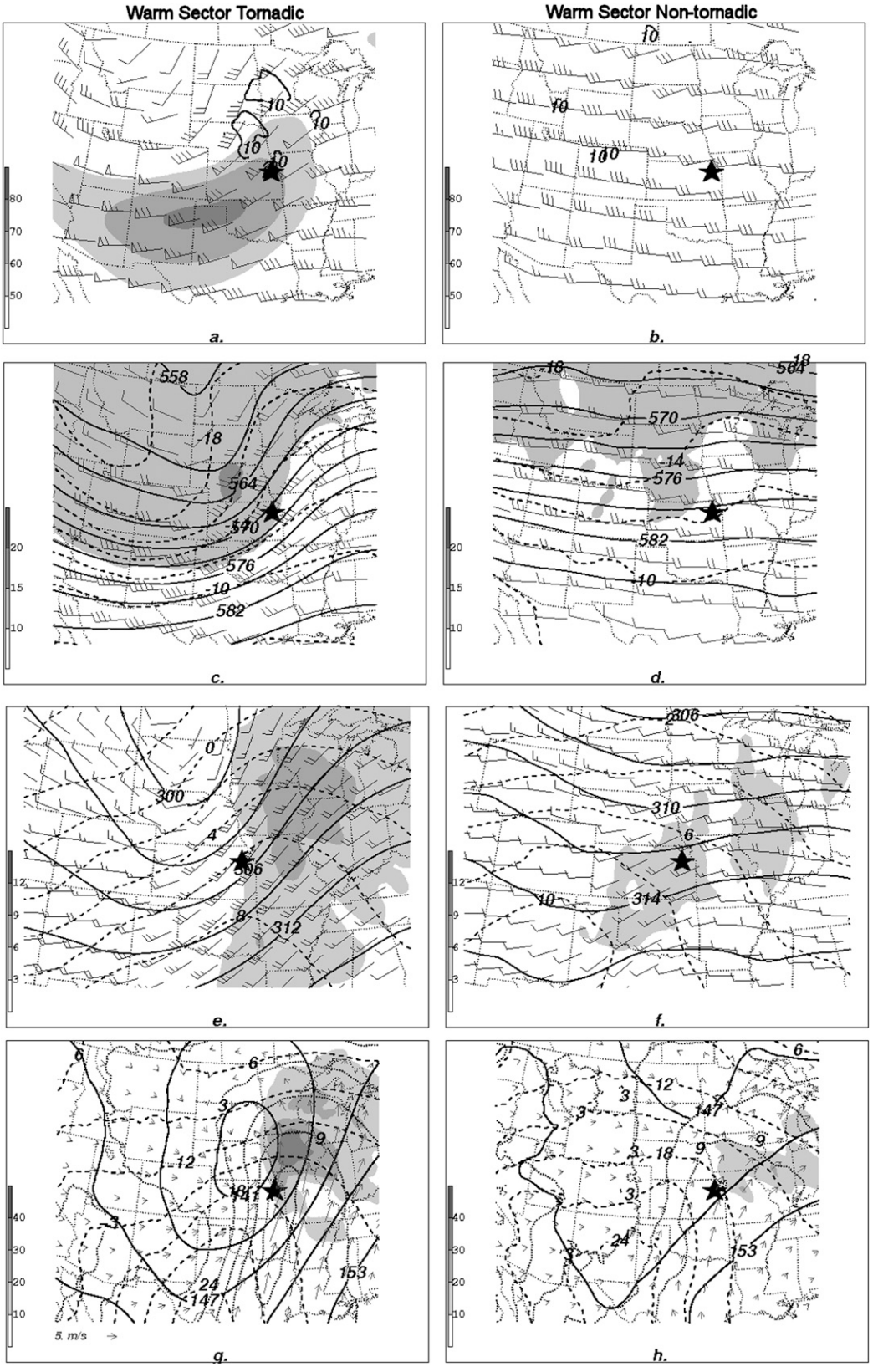

FIG. 7. As in Fig. 2, but for (left) warm sector tornado and (right) null warm sector null events.

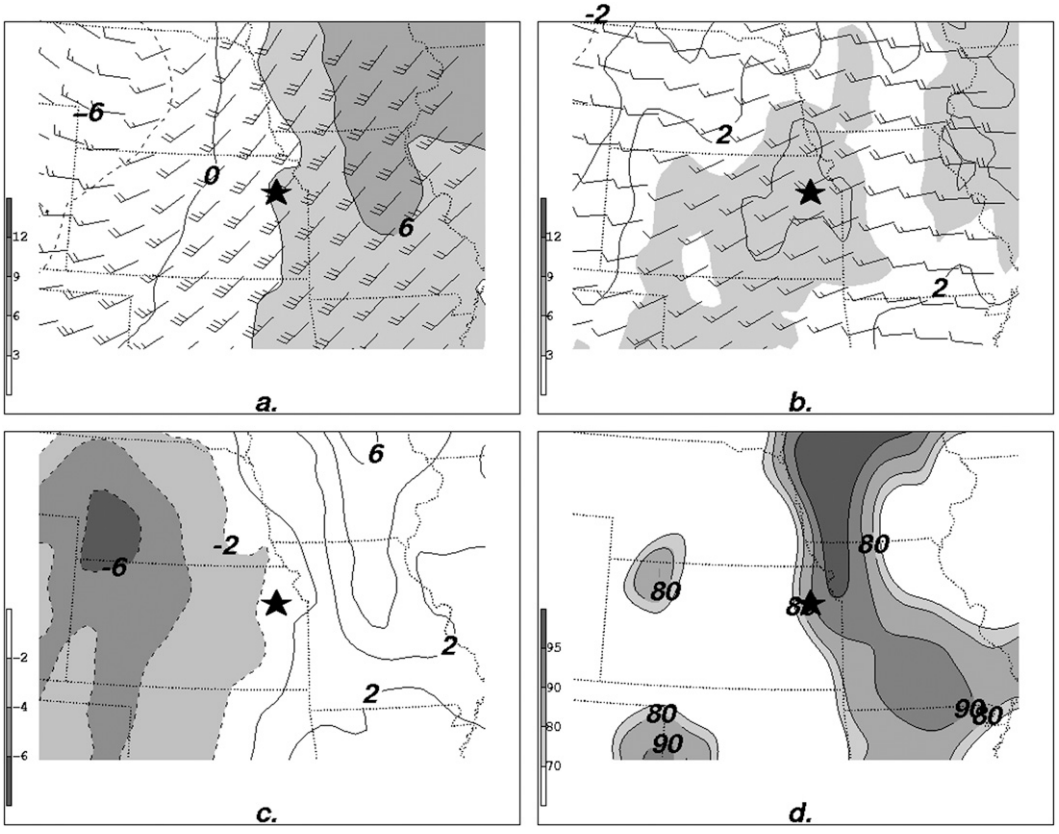

FIG. 8. As in Fig. 4, but for 700-hPa temperature advection [K (12 h)$^{-1}$] for warm sector (a) tornado and (b) null cases. Wind barbs are in meters per second (half barb is equal to 2.5 m s^{-1} and a full barb is 5 m s^{-1}).

surface trough. The composite location of the significant tornado is near the western edge of the MUCAPE axis, while the nontornadic warm sector composite had less MUCAPE over a broader area with similar values of MUCIN (Figs. 12c and 12d).

For MLLCL heights, the most striking difference was between boundary tornadoes and null boundary events, where little overlap of inner quartiles was noted (Fig. 11b). Differences in the mean values of MLLCL in distinguishing tornadic and nontornadic environments have been identified in other studies as well (RB98, CB04, T03, G12). The means of the RUC MLLCL were lower than in the NARR for both boundary datasets, with values similar to previous significant tornado studies (RB98, CB04, Thompson et al. 2012). Although not as prominent, a statistically significant difference was found in the means between the warm sector and null warm sector. The height of the MLLCL for warm sector significant tornadoes was noticeably higher than observed in previous studies but is was consistent for both the NARR and RUC datasets, potentially indicating a higher MLLCL is favored in this region of the Great Plains. The overlap in the inner quartiles of the box-and-whiskers plots of the warm sector events in both the NARR and RUC may indicate less of an effective tool for distinguishing warm sector significant tornadoes to null events.

The differences in the means of the MLLFC height also were significant for both boundary and warm sector events (Fig. 11c), with little inner-quartile overlap of the box-and-whisker plots for the NARR data. Unlike MLLCL, the means of MLLFC heights in the NARR reanalysis were lower than those in the RUC. The NARR MLLFC mean values were similar to those found by Davies (2004) for F2–F4 tornadoes. Garner (2012) did not find significant differences in MLCAPE, MLCIN, and MLLCL, but that study compared significant to weak tornadoes in the warm sector and boundary environments and did not include a null tornado database.

The kinematic parameters of 0–1- and 0–3-km SRH using the internal dynamics storm motion (Bunkers et al. 2000); 0–1-, 0–3-, and 0–6-km bulk wind difference (BWD); and storm-relative winds (SRWs) from 0–1, 0–3, 5, 8, and 7–10 km were calculated. Consistent with previous studies indicating higher SRH is often observed with greater tornado potential (Thompson et al. 2012; T03, CB04, RB98), the 0–1- and 0–3-km SRH

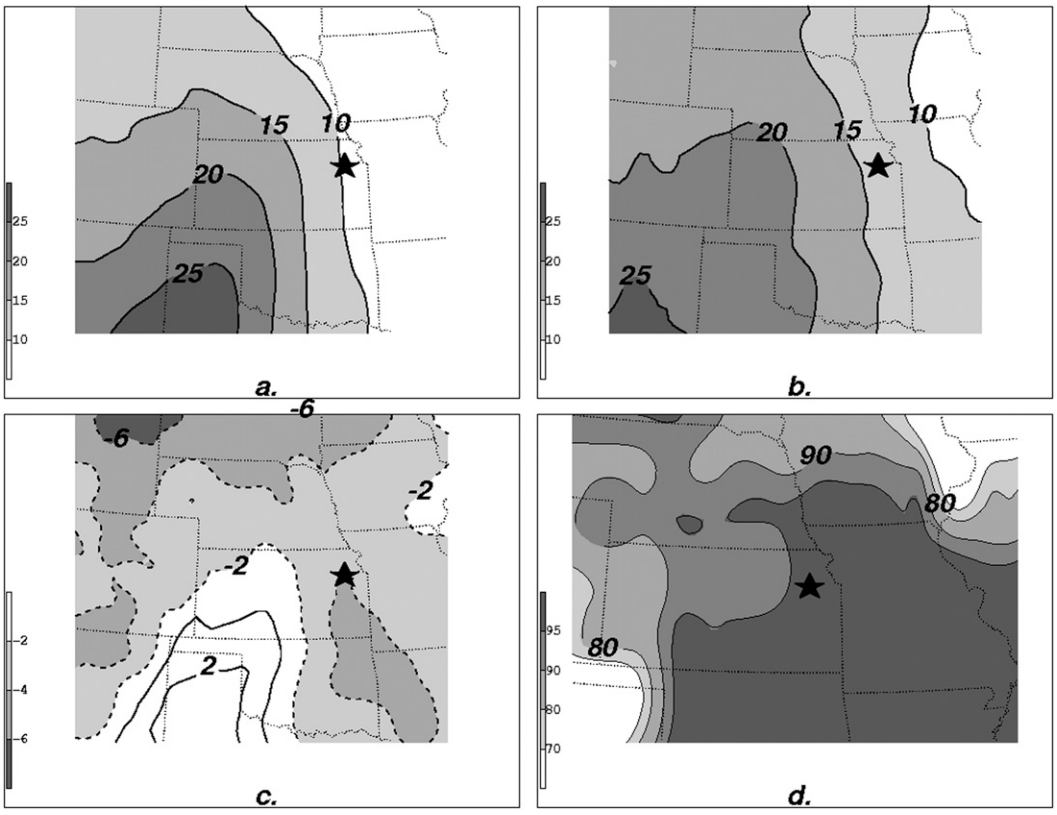

FIG. 9. As in Fig. 4, but for 2-m dewpoint depression (°C) for warm sector (a) tornado and (b) null cases. Shaded every 5°C for values >10°C.

(Figs. 13a and 13b) were statistically higher for both boundary and warm sector tornado events compared to their respective null events. Similar to SRH, the difference in the means of the 0–1-km BWD were significantly higher in both boundary and warm sector tornado events than their respective null cases (Fig. 13c). This is especially evident in the warm sector comparison, where little inner-quartile overlap was noted, which may indicate that 0–1-km BWD has more utility in distinguishing between warm sector tornadic and nontornadic events

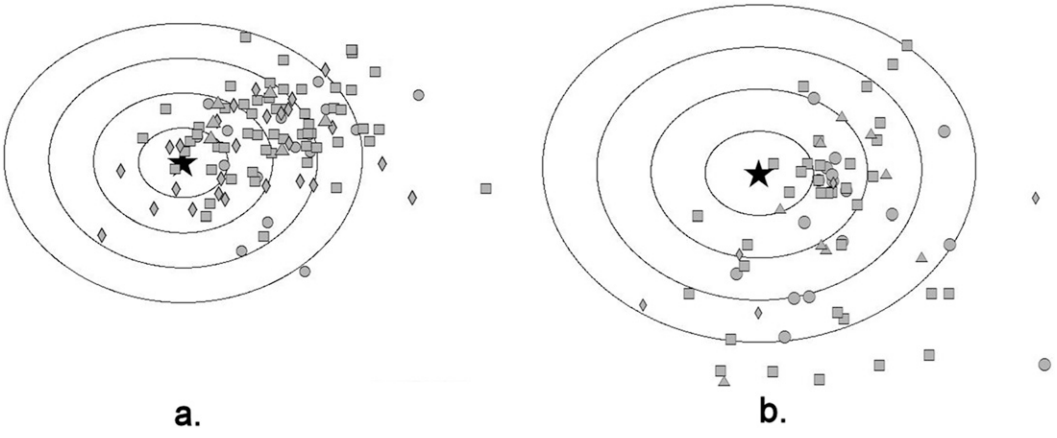

FIG. 10. Surface-low-relative tornado plots for (a) boundary and (b) warm sector significant tornadoes. Solid star represents the system-relative minimum in sea level pressure. Circles represent events from January to April, squares are for May to June, diamonds are for July to August, and triangles are for September to December. Range rings are shown every 150 km.

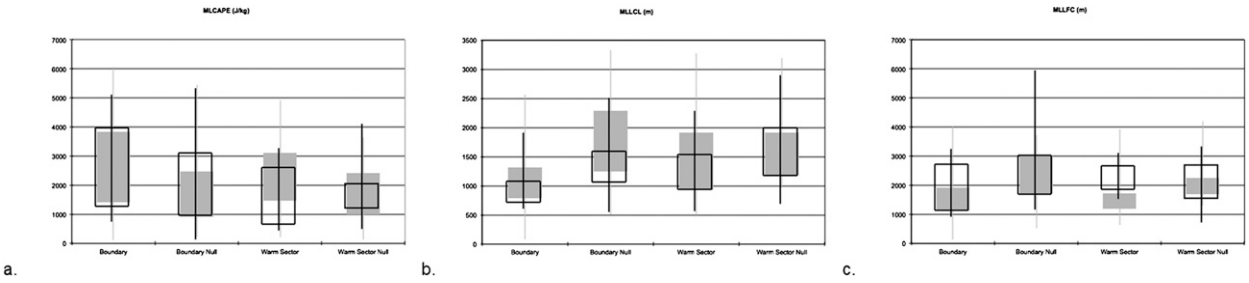

FIG. 11. Standard box-and-whiskers plots for (a) MLCAPE ($J\,kg^{-1}$), (b) MLLCL (m), and (c) MLLFC (m). NARR is shown by light gray shading, and RUC is shown in solid black. The shaded box encloses the 25th–75th percentiles, while the whiskers extend to the maximum and minimum values.

than boundary events. Similar results for the warm sector were noted in the 0–3-km BWD (Fig. 13d), but unlike the 0–1-km BWD, the boundary events also indicated little inner-quartile overlap in the 0–3-km layer. This may suggest that 0–3-km BWD has more operational utility in distinguishing the tornado potential near boundaries than does the 0–1-km BWD. Although the 0–6-km BWD for both boundary and warm sector tornado events was higher than the null cases, all datasets had mean values $>15\,m\,s^{-1}$ that have been found to be associated with supercells (Fig. 13e; M98, RB98, Bunkers 2002). This is likely a result of only including radar-observed supercells for the null cases. Nevertheless, both the boundary and warm sector tornado means were statistically higher than the nontornadic databases, indicating some operational utility. When the distribution of 0–1-km SRH and MLCAPE are plotted, similar patterns for both boundary and warm sector events are apparent (Fig. 14). Both

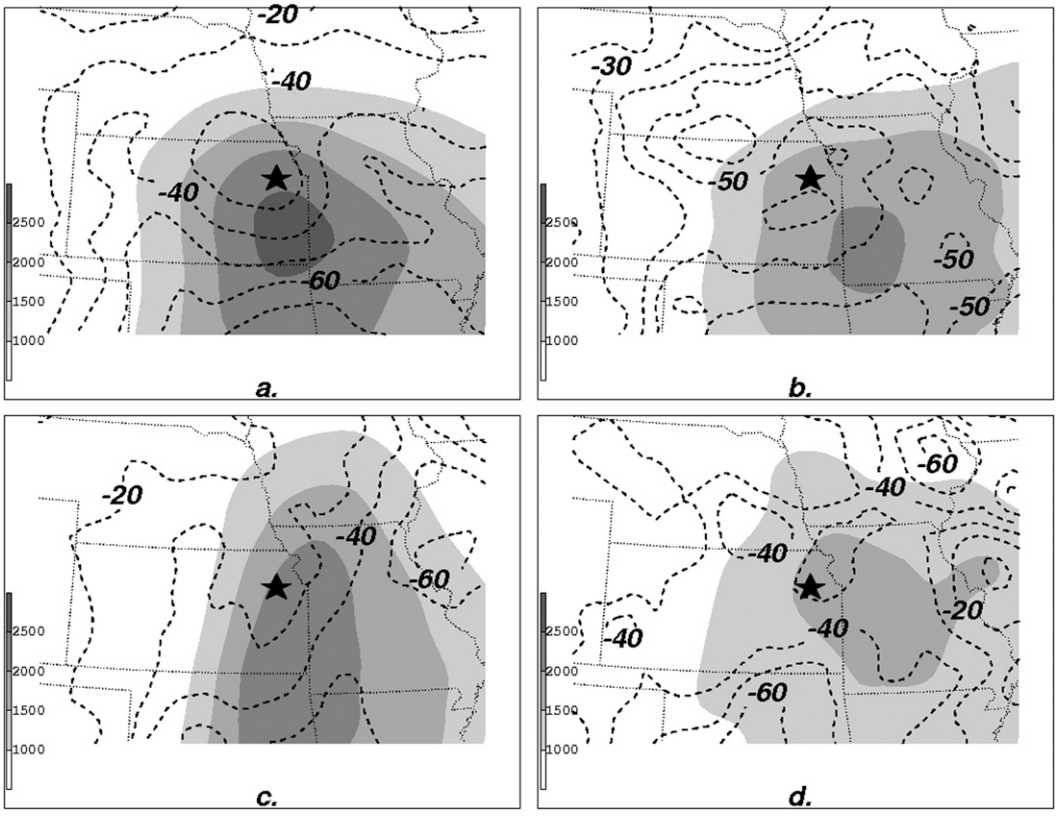

FIG. 12. Composite analysis of MUCAPE shaded every 500 $J\,kg^{-1}$ for values $> 1000\,J\,kg^{-1}$ and MUCIN dashed contours every 10 $J\,kg^{-1}$ for (a) boundary significant tornado events, (b) nontornadic boundary events, (c) warm sector significant tornado, and (d) nontornadic warm sector events.

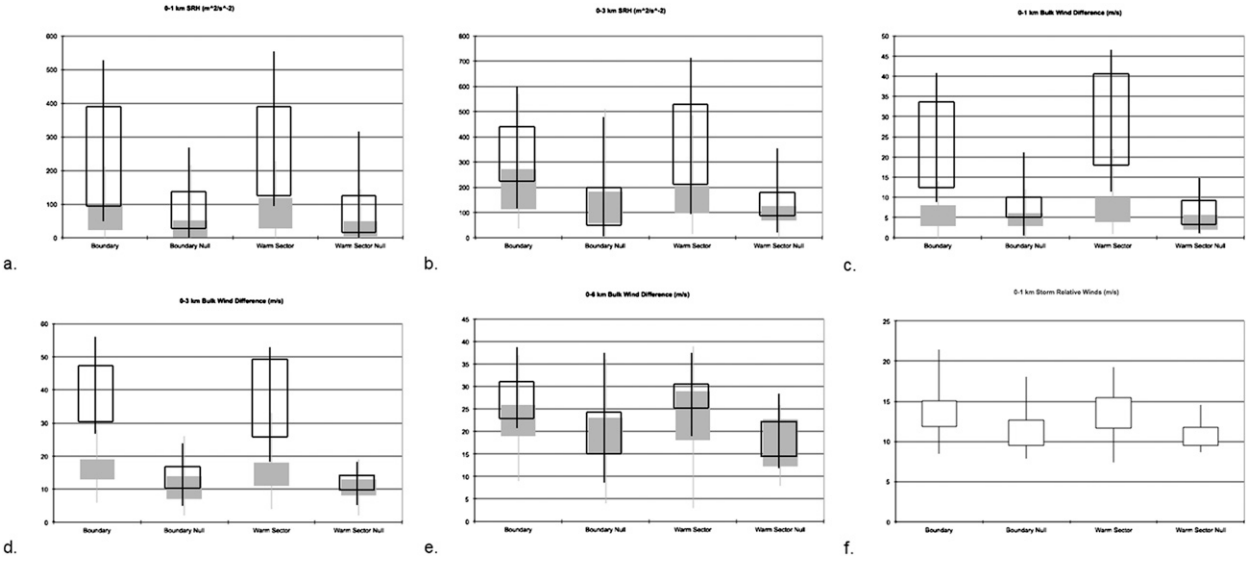

FIG. 13. As in Fig. 11, but for (a) 0–1-km SRH ($m^2 s^{-2}$), (b) 0–3-km SRH ($m^2 s^{-2}$), (c) 0–1-km BWD ($m s^{-1}$), (d) 0–3-km BWD ($m s^{-1}$), (e) 0–6-km BWD ($m s^{-1}$), and (f) 0–1-km SRW ($m s^{-1}$).

nontornadic datasets generally had less 0–1-km SRH than the tornado events, but the MLCAPE in the nontornadic warm sector cases displayed more variability than nontornadic boundary cases.

For all 0–1- and 0–3-km SRH, as well as 0–1- and 0–6-km BWD, the NARR values were lower than were observed with the RUC. RUC values of SRH and BWD were closer to those observed in previous studies (RB98, CB04, Thompson et al. 2012). Although beyond the scope of this study, differences appear to be associated with weaker than observed wind speeds near and below 1 km in the NARR when compared to the RUC. The lower SRH and BWD values significantly limit the transfer of NARR values of these parameters to operations. That said, similar variances in the means of SRH and BWD did indicate that the NARR does have skill in discriminating significant boundary and warm sector tornadoes from null events, and those relationships can translate to operations.

Brooks et al. (1994) examined the role of SRW through numerical modeling, finding that SRWs were important to the development of a low-level mesocyclone by controlling the distribution of precipitation within the supercell. Although Thompson (1998) found that SRWs near 500 hPa could help differentiate tornadic and nontornadic supercell environments, later studies did not find a statistically significant relationship throughout the atmosphere (Markowski et al. 2003; T03). Although research results have varied, it appears that SRW may be a good discriminator between boundary and warm sector significant tornado events and their respective nontornadic cases. The differences in the means in the 0–1-km layer appeared to have the most utility for both boundary and warm sector events, with little interquartile overlap noted in the box-and-whiskers plots (Fig. 13f). Statistically significant differences in SRW were also noted for the warm sector at 0–3, 5, and 8 km (not shown). This suggests that for the warm sector significant tornadoes, SRW through a deeper layer may be more important than in the boundary cases, in which no other layer tested proved to be significant. Although not tested, consistent with SRH and BWD, the values of NARR likely have a low bias, especially for low-level SRW. Thus, as with SRH and BWD, the difference in the means of the NARR SRW has significance, but specific values have limited ability to be transferred directly to operations.

Low-level lapse rates also appear to play a significant role in distinguishing between both boundary and warm sector significant tornado events and their respective null cases. Davies (2006) showed that for F1–F4 tornadoes that have an LCL below 1300 m and SRH $> 75\ m^2 s^{-2}$, the lapse rate in the 0–2-km layer is significantly lower than F1–F4 tornadoes, with higher LCL heights and lower SRH. CB04 found that for significant tornadoes, the low-level lapse rate was lower than for thunderstorms with significant hail or wind. They attributed the lower lapse rate to the likely presence of additional low-level moisture in tornado environments and thus less boundary layer mixing. Analysis of the 0–2-km lapse rates for both the boundary and warm sector events in this study produced similar results. In the boundary significant tornado

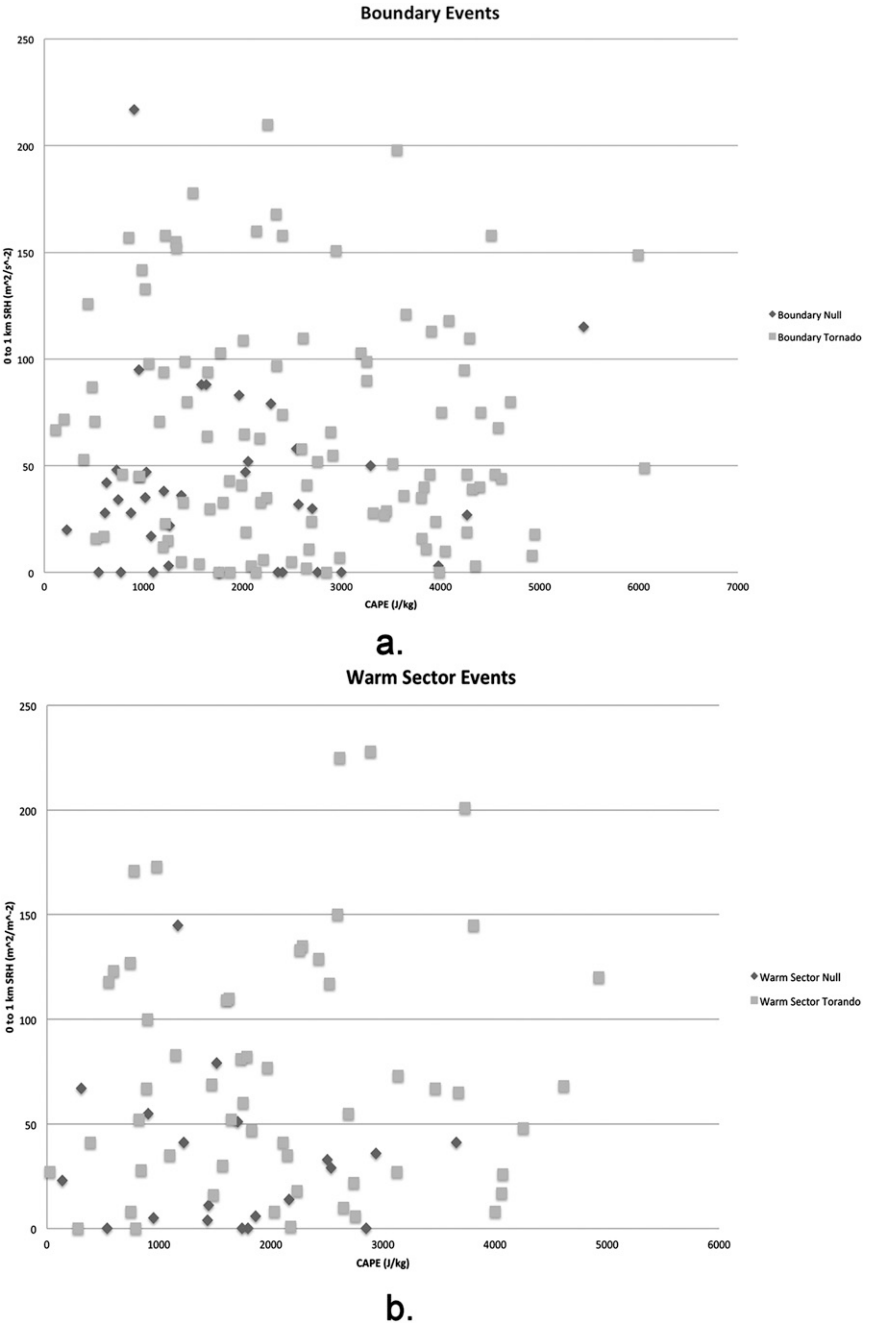

FIG. 14. Scatterplot of MLCAPE ($J\,kg^{-1}$) and 0–1-km SRH ($m^2\,s^{-2}$) for (a) boundary and (b) warm sector events. Black diamonds are nontornadic events and gray squares are significant tornadic events.

composite, tornadogenesis was just east of the steepest low-level lapse rates (Fig. 15). The null boundary composite indicated that the events tended to occur within the axis of highest low-level lapse rates. These differences were significant not only at the composite event location, but also downstream. Similar results were seen in the warm sector composite as well (Fig. 16). For the warm sector significant tornado composite, the 0–2-km lapse rates were steeper than in the boundary significant tornado composite, but the tornadogenesis location was near the eastern edge of the steepest lapse rates, with lower values found downstream to the east as in the boundary tornado event composite. Also similar to the boundary composites, the null warm sector events had

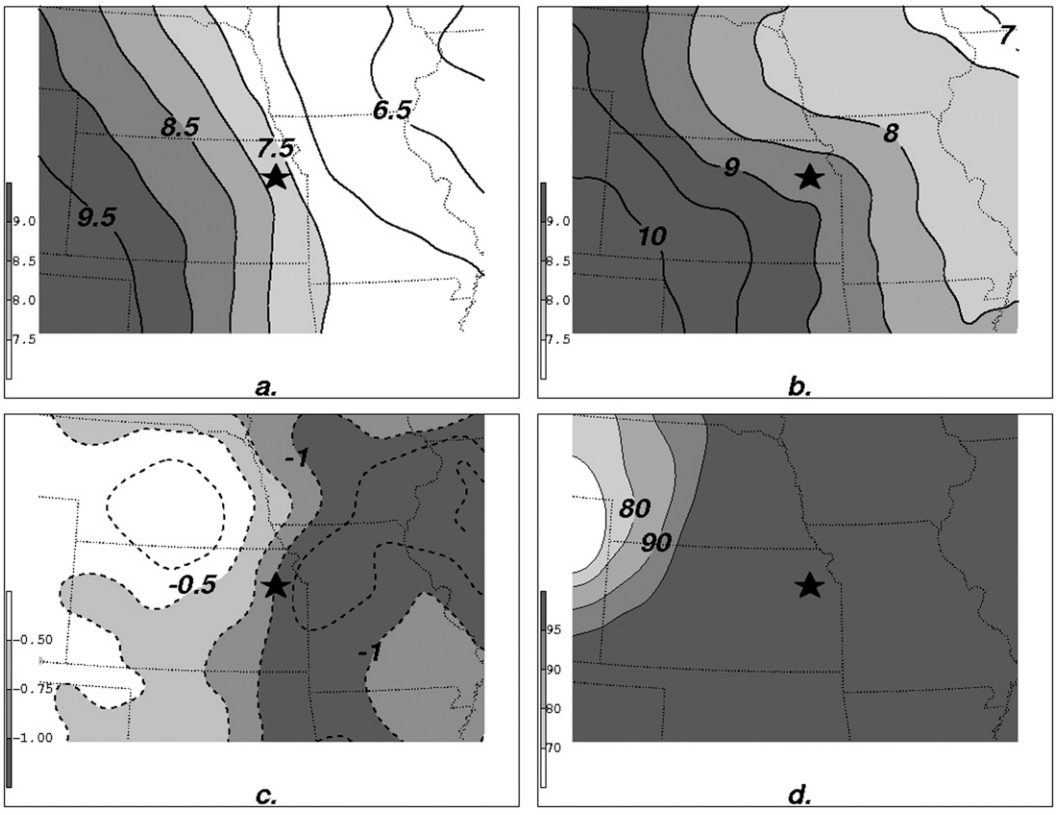

FIG. 15. As in Fig. 4, but for boundary 0–2-km lapse rate (°C km^{-1}) for boundary (a) tornado and (b) null events, contoured every 0.5°C km^{-1} and shaded for values > 7.5°C km^{-1}.

a significantly steeper low-level lapse rate near and downstream of the report location.

Several studies have shown the importance of low CIN values associated with tornadoes (RB98, CB04, Davies 2004; Mead and Thompson 2011). Garner (2012) found that MLCIN was not a good discriminator for comparing significant to weak warm sector (boundary) tornadoes. Similar results using MUCIN were found in this study for warm sector events (not shown). Differences in MUCIN were more noticeable in comparing the boundary composites (Fig. 17). MUCIN near the composite location of the tornado and points to the west showed significantly lower values than in the null composite. The values for the boundary tornado and null boundary composites were similar to the results found by RB98. The area of greatest difference in the MUCIN composite values was along and north of the surface boundary where the null composite indicated deformation and confluence in the surface wind field (Fig. 5).

The presence of a low-level jet (Holton 1967; Bonner 1966) that results in stronger 0–1-km BWD has been shown to be associated with significant tornadoes (CB04, Schumacher and Boustead 2011; Mead and Thompson 2011). Similar to Garner (2012), significant differences appeared in the 0–1-km BWD when comparing boundary and warm sector tornado events to their respective null cases. In the boundary tornado composite, the tornado occurred along the western edge of the greatest 0–1-km BWD, and the BWD was stronger than the null boundary composite along this axis and areas to the east (Fig. 18). Even larger differences in 0–1-km BWD were noted in the warm sector composites (Fig. 19). Similar to the boundary tornado composite, the location of tornadogenesis was near the western edge of the highest axis of BWD. The values of BWD in the warm sector tornado composite were double that of the null cases in many areas near and downstream of the composite location of the event. The values of 0–1-km BWD for the warm sector were similar to those found by G12 to be associated with southern plains spring tornadoes, while the boundary tornado values were closer to the northern plains summer tornadoes shown by G12.

Analysis of composite soundings and ground-relative hodographs revealed many of the previously mentioned differences between boundary and warm sector events and their respective null cases (Fig. 20). The soundings indicated that the tornado composites were moister below 800 hPa than the null composites, leading to lower

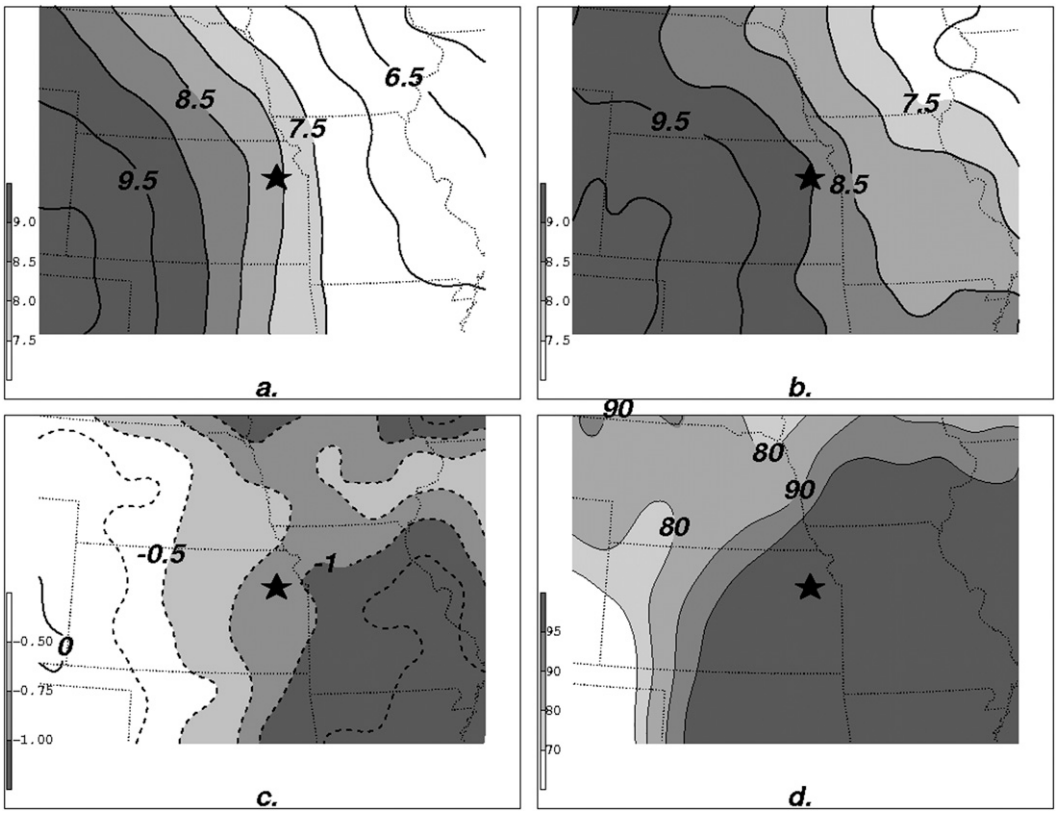

FIG. 16. As in Fig. 15, but for the warm sector.

LCL heights and more stable 0–2-km lapse rates. The tornado soundings indicated drier air between 700 and 300 hPa than did the null composite soundings. The composite hodographs for the boundary tornado and null boundary events were similar in both shape and length. Consistent with the clustering of the significant tornado reports associated with the boundary tornadoes northeast of the area of lowest sea level pressure, the hodograph is similar to those shown by Bluestein and Banacos (2002) for events in the northeast quadrant of surface cyclones. The similarities of the boundary hodographs may suggest that the differences between the boundary tornado and null events may be more thermodynamic than kinematic, with the 0–2-km lapse rates, lower low-level dewpoint depressions, and effects of the confluence and deformation along the boundary playing the largest roles (Fig. 20a). Although thermodynamic and synoptic differences between warm sector tornadoes and null warm sector events played a significant role, there were also differences in the composite hodographs (Fig. 20b). The lighter environmental winds were apparent in the null warm sector composite hodograph, while the warm sector tornado composite hodograph was longer and exhibited more shear throughout the atmosphere. The clustering of the significant warm sector tornado reports from the east through the southwest of the area of low pressure are similar to the results from Bluestein and Banacos (2002) for hodographs in the southeast quadrant of a surface cyclone. Although the composite hodograph of the null warm sector events (Fig. 20b) was in the top-right quadrant of the hodograph, the presence of the cyclonic midlevel curvature resembles some aspects of the Bluestein and Banacos (2002) hodographs associated with anticyclones as well.

4. Conclusions

This study compares the environments that produce significant tornadoes associated with a boundary to supercells within close proximity to boundaries that fail to produce a tornado, as well as significant tornadoes in the free warm sector to supercells in the free warm sector that fail to produce a significant tornado, for a part of the central and northern Great Plains. The study includes significant tornadoes for the period 1979–2011 for this area. Using subjective surface analyses, each event was classified as occurring either near a discernible boundary or in the warm sector. Using NARR data, system-relative

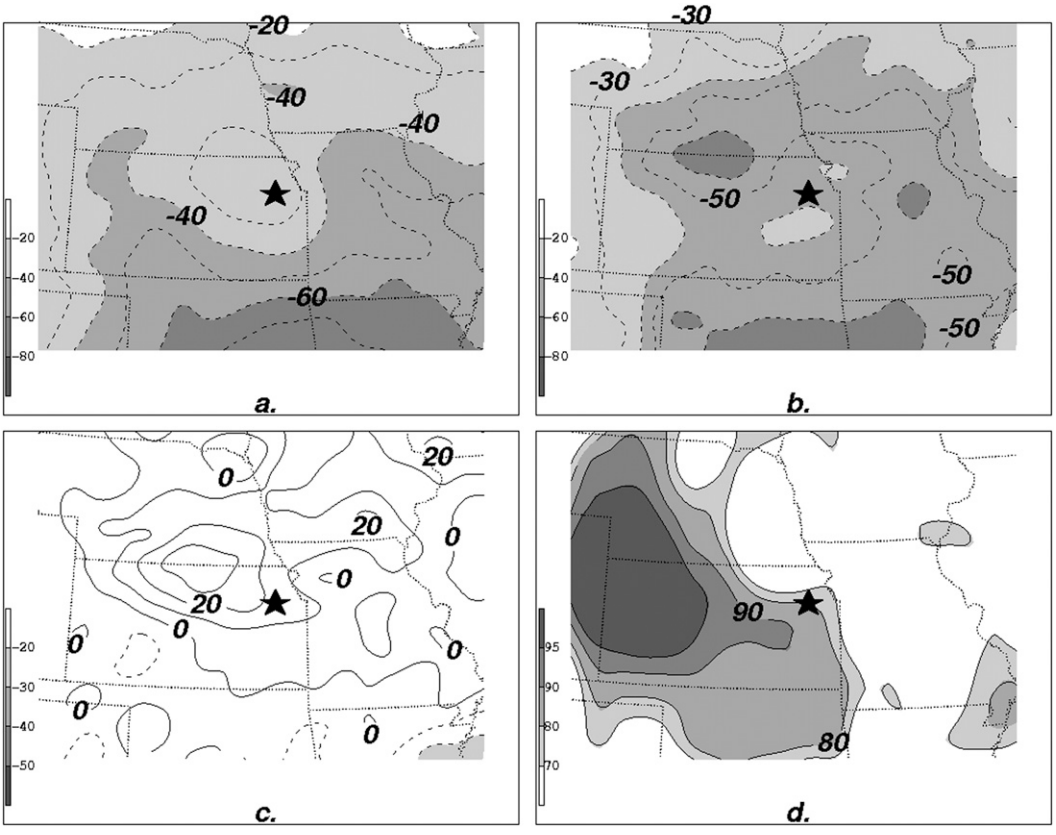

FIG. 17. As in Fig. 4, but for boundary SBCIN ($J\,kg^{-1}$), with dashed contours every $10\,J\,kg^{-1}$ and shaded for values $<-20\,J\,kg^{-1}$.

composites were developed for each group of events. Several synoptic-scale environmental characteristics were compared, and the WMW statistical significance test was used to determine if the differences observed were meaningful. The climatology of these events was compared, and the Student's *t* test was used to determine the significance of these differences. The NARR data were analyzed using NSHARP to investigate the convective environment for the grid point nearest the location of tornadogenesis or the hail report. Additionally, for the period of the study from 2005 through 2011, RUC data were obtained from the SPC and compared to the NARR data to provide values of convective parameters that can be applied directly to operations.

A comparison of the length, width, hour of day, and date was made between the boundary and warm sector significant tornadoes. The only significant difference in the means was in the pathlength of the warm sector tornadoes over boundary tornadoes. The warm sector significant tornado event varied more in path width than did the boundary significant tornado events, and the warm sector tornado events occurred more often during the peak tornado season than did boundary tornado events. The boundary tornado events tended to happen through a wider range of the day, while the warm sector events were largely confined to the afternoon and evening.

Analysis of the data provided a number of key indicators that can help operational forecasters distinguish between environments that are likely to produce significant tornadoes along boundaries to those that are less likely. Both composites indicated a 300-hPa jet maximum downstream of the report location, but in the null environments, this jet occurred in closer proximity to the report than in the significant tornado composite. The closer proximity of the downstream jet appeared to lead to an ageostrophic frontal circulation in the entrance region of this jet that resulted in significant differences in the surface composite. At the surface, the effects of the downstream jet led to stronger confluence into the boundary and significantly stronger deformation near the report location in the null cases. The boundary significant tornado composite lacked the close proximity of the downstream jet, but was located near the exit region of an upstream jet streak and showed minimal confluence of the surface winds into the boundary. Due to the more neutral orientation of the short-wave trough in the

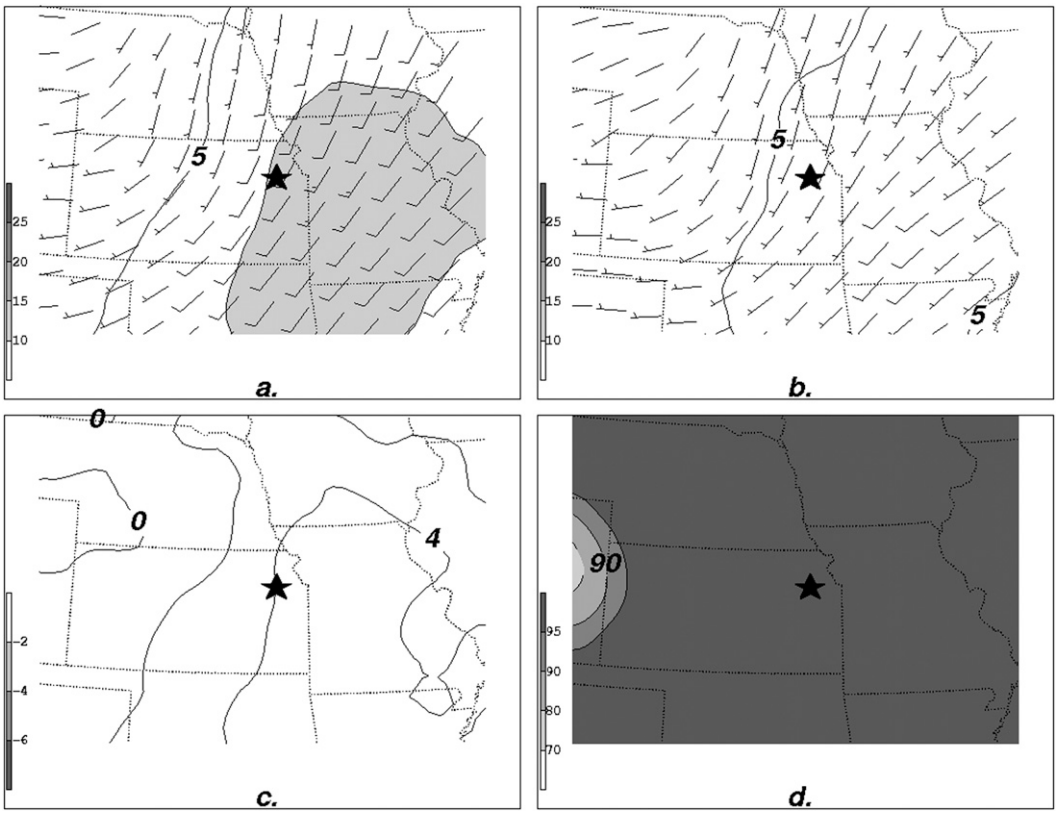

FIG. 18. As in Fig. 4, but for boundary 0–1-km BWD ($m\,s^{-1}$), contoured every $5\,m\,s^{-1}$ with values $>10\,m\,s^{-1}$ shaded. Wind barbs are in meters per second (half barb is equal to $2.5\,m\,s^{-1}$ and a full barb is $5\,m\,s^{-1}$).

boundary tornado composite, compared to the positive tilt of the null composite, the low-level temperature and moisture advection also appeared to be significantly higher. The higher influx of low-level moisture appeared to lead to more stable 0–2-km lapse rates and lower surface dewpoint depressions from the tornadogenesis location and points to the east that were statistically significant compared to the null events.

The differences in the synoptic environment between the warm sector tornado and null events were more striking than in the boundary comparison. Because warm sector events are synoptically evident, the differences may be apparent with greater forecast lead time than boundary cases, which may be more driven by the mesoscale environment along the frontal boundary. The warm sector tornado composite indicated that these events were synoptically evident and occurred with a pronounced upper-level trough associated with a cyclonically curved 300-hPa jet, with the tornadogenesis location in the exit region and a negatively tilted midlevel short-wave trough with increasing values of absolute vorticity upstream of the tornadogenesis location. In contrast, the null warm sector composite showed a west-to-northwest flow pattern that was substantially less amplified than in the tornado composite. A short-wave trough was noted in the null composite, but the report location was located near the southern edge of the forcing for ascent associated with this trough. While the tornado composite indicated the tornadogenesis location was near the zero 700-hPa temperature advection line, the null composite indicated WAA occurring near the report location. Similar to the boundary events, the warm sector tornado composite had significantly more low-level moisture, leading to a lower dewpoint depression and more stable 0–2-km lapse rates. In both the boundary and warm sector tornado composites, tornadogenesis occurred along the eastern edge of the steeper 0–2-km lapse rates, but the gradient upstream from the location was steeper in the warm sector cases.

Specific values of NARR thermodynamic and kinematic parameters yielded less operational utility for both boundary and warm sector events compared to previous studies. Although a statistical comparison of NARR and RUC was not completed for this study, evidence indicates the NARR may contain a low wind speed bias near and below 1 km. While specific values of some

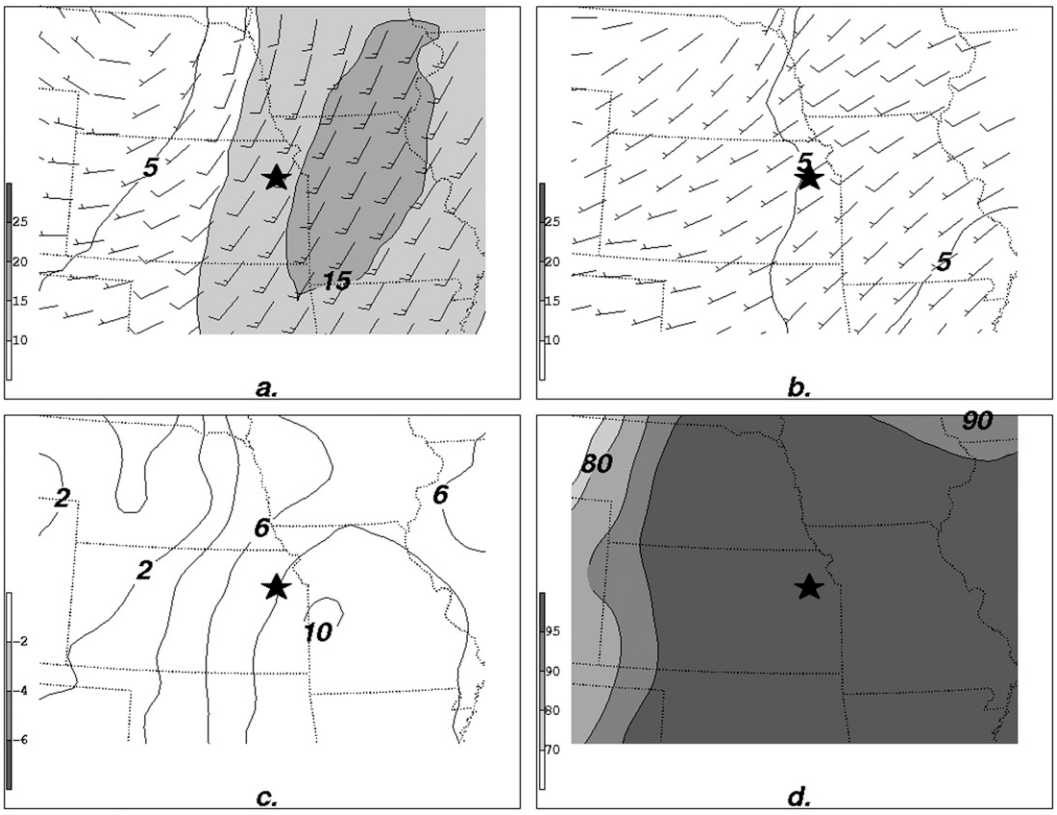

FIG. 19. As in Fig. 18, but for the warm sector.

thermodynamic and kinematic parameters lack the ability to be directly transferred to operations, statistical significant differences in the means of these values do have operational importance in discriminating significant boundary (warm sector) tornadoes from nontornadic boundary (warm sector) events. This was shown when the NARR was compared to the RUC, as the difference in the means between significant tornadoes and the null cases was similar.

While disparities in the synoptic pattern of the boundary events were smaller compared to the warm sector, significant differences occurred in the thermodynamic parameters of MLLCL and MLLFC, where limited overlap in the inner quartiles was noted in the box-and-whiskers diagrams. The kinematic parameters 0–1- and 0–3-km SRH and BWD, as well as 0–1-km SRW, also proved to be significant. The parameters of 0–3-km BWD and SRH, as well 0–1-km SRW, showed the least inner-quartile overlap. This suggests that low-level thermodynamic and kinematic parameters, combined with the degree of deformation in the right-rear entrance region of the downstream jet, may produce the best utility for distinguishing significant boundary tornado events from nontornadic boundary events.

Analysis of warm sector convective thermodynamic and kinematic parameters also yielded important differences relevant to operational forecasting. Past studies have indicated MLLCL and MLLFC as discriminators for tornadoes, and although statistically significant differences were observed in this dataset, overlap of the inner quartiles of the box-and-whiskers plots may indicate less of a discriminating value between significant tornado and null events for this part of the central and northern Great Plains. All kinematic parameters tested for the warm sector events proved to be significant with little inner-quartiles overlap, especially low-level BWD, SRH, and SRW, suggesting that these, along with the differences in the synoptic patterns, appeared to have the best discriminating value.

The composites presented will not cover every significant tornado event possible in this segment of the Great Plains. The goal of the research was to help identify key differences in the environment that can help distinguish situations that will likely support significant tornadoes along boundaries or in the warm sector from those that are less likely. In this study, several key discriminators have been identified to move toward that goal.

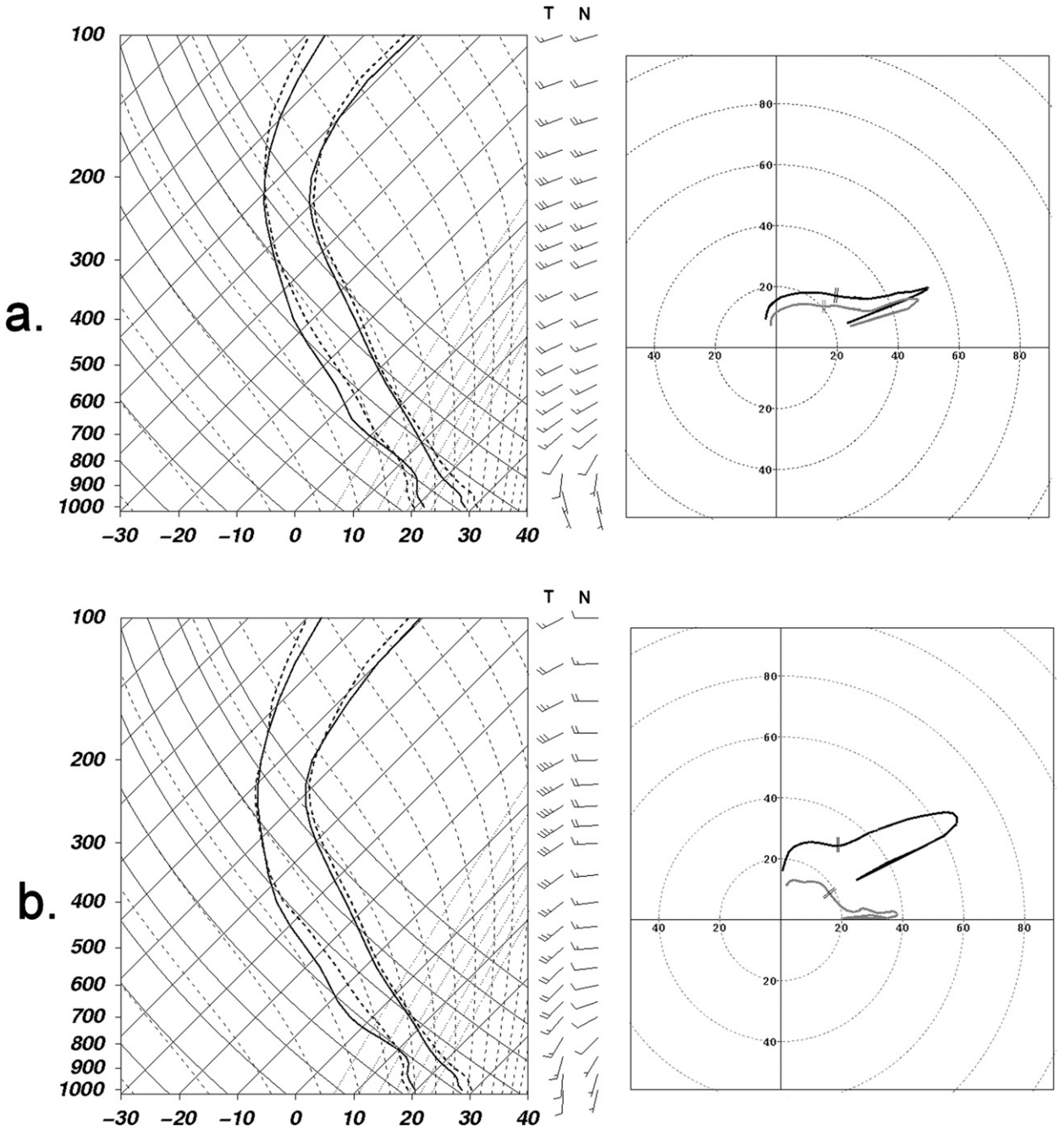

FIG. 20. Composite skew T–log$p$ diagrams and hodographs for (a) boundary tornado (solid black skew T and hodograph) and null (dashed skew T and gray hodograph), and for (b) warm sector tornado (solid black skew T and hodograph) and null (dashed skew T and gray hodograph). Winds are in m s^{-1} (half barb is equal to 2.5 m s^{-1} and a full barb is 5 m s^{-1}). Scalloping in the hodographs indicates the top of the 3-km layer.

Acknowledgments. The authors thank Rebecca Kern (National Weather Service, Omaha/Valley, Nebraska) for assistance with several map graphics. We are grateful to Charles Graves of Saint Louis University for use of the GEMPAK compositing program. We are also appreciative of Jared Guyer and Andy Deans (Storm Prediction Center) for providing archived Storm Prediction Center RUC data. Two anonymous reviewers provided insightful commentary that improved the quality of this manuscript.

REFERENCES

Atkins, N. T., M. L. Weisman, and L. J. Wicker, 1999: The influence of preexisting boundaries on supercell evolution. *Mon. Wea. Rev.,* **127,** 2910–2927.

Beebe, R. G., and F. C. Bates, 1955: A mechanism for assisting in the release of convective instability. *Mon. Wea. Rev.,* **83,** 1–10.

Benjamin, S. G., J. M. Brown, K. J. Brundage, B. E. Schwartz, T. G. Smirnova, T. L. Smith, and L. L. Morone, 1998: RUC-2 - The Rapid Update Cycle version 2. NWS Tech. Procedures Bull. 448, 18 pp. [Available online at www.nws.noaa.gov/om/tpb/448.pdf.]

Bluestein, H. B., and P. C. Banacos, 2002: The vertical profile of the wind and temperature in cyclones and anticyclones over the eastern two-thirds of the United States: A climatology. *Mon. Wea. Rev.,* **130,** 477–506.

Bonner, W. D., 1966: Case study of thunderstorm activity in relation to the low-level jet. *Mon. Wea. Rev.,* **94,** 167–178.

Bothwell, P. D., J. Hart, and R. L. Thompson, 2002: An integrated three-dimensional objective analysis scheme in use at the Storm Prediction Center. Preprints, *21st Conf. on Severe Local Storms/19th Conf. on Weather Analysis and Forecasting/15th Conf. on Numerical Weather Prediction,* San Antonio, TX, Amer. Meteor. Soc., JP3.1. [Available online at https://ams.confex.com/ams/pdfpapers/47482.pdf.]

Brooks, H. E., C. A. Doswell III, and R. B. Wilhelmson, 1994: The role of midtropospheric winds in the evolution and maintenance of low-level mesocyclones. *Mon. Wea. Rev.,* **122,** 126–136.

Bunkers, M. J., 2002: Vertical wind shear associated with left-moving supercells. *Wea. Forecasting,* **17,** 845–855.

——, B. A. Klimowski, J. W. Zeitler, R. L. Thompson, and M. L. Weisman, 2000: Predicting supercell motion using a new hodograph technique. *Wea. Forecasting,* **15,** 61–79.

——, M. R. Hjelmfelt, and P. L. Smith, 2006: An observational examination of long-lived supercells. Part I: Characteristics, evolution, and demise. *Wea. Forecasting,* **21,** 673–688.

——, J. R. Wetenkamp Jr., J. J. Schild, and A. Fischer, 2010: Observations of the relationship between 700-mb temperature and severe weather reports across the contiguous United States. *Wea. Forecasting,* **25,** 799–814.

Clark, A. J., C. J. Schaffer, W. A. Gallus Jr., and K. Johnson-O'Mara, 2009: Climatology of storm reports relative to upper-level jet streaks. *Wea. Forecasting,* **24,** 1032–1051.

Coniglio, M. C., J. Y. Hwang, and D. J. Stensrud, 2010: Environmental factors in the upscale growth and longevity of MCSs derived from Rapid Update Cycle analysis. *Mon. Wea. Rev.,* **138,** 3514–3539.

Corfidi, S. F., S. J. Weiss, J. S. Kain, S. J. Corfidi, R. M. Rabin, and J. J. Levit, 2010: Revisiting the 3–4 April 1974 Super Outbreak of tornadoes. *Wea. Forecasting,* **25,** 465–510.

Craven, J. P., and H. E. Brooks, 2004: Baseline climatology of sounding derived parameters associated with deep moist convection. *Natl. Wea. Dig.,* **28,** 13–24.

Davies, J. M., 2004: Estimations of CIN and LFC associated with tornadic and nontornadic supercells. *Wea. Forecasting,* **19,** 714–726.

——, 2006: Tornadoes in environment with small helicity and/or high LCL heights. *Wea. Forecasting,* **21,** 579–594.

Davies-Jones, R. P., D. Burgess, and M. Foster, 1990: Test of helicity as a tornado forecasting parameter. Preprints, *16th Conf. on Severe Local Storms,* Kananaskis Park, AB, Canada, Amer. Meteor. Soc., 558–592.

desJardins, M. L., K. F. Brill, and S. S. Schotz, 1991: GEMPAK5 user's guide, version 5.0. NASA Tech. Memo. NASA TM-4260, 232 pp. [Available from NASA, Code NTT-4, Washington, DC 20546-0001.]

Doswell, C. A., III, 1980: Synoptic-scale environments associated with high plains severe thunderstorms. *Bull. Amer. Meteor. Soc.,* **61,** 1388–1400.

——, 1987: The distinction between large-scale and mesoscale contribution to severe convection: A case example. *Wea. Forecasting,* **2,** 3–16.

——, S. J. Weiss, and R. H. Johns, 1993: Tornado forecast: A review. *The Tornado: Its Structure, Dynamics, Prediction and Hazards, Geophys. Monogr.,* Vol. 79, Amer. Geophys. Union, 557–571.

Dowdy, S., S. Wearden, and D. Chilko, 2004: *Statistics for Research.* 3rd ed. Wiley-Interscience, 640 pp.

Gaffin, D. M., and S. S. Parker, 2006: A climatology of synoptic conditions associated with significant tornadoes across the southern Appalachian region. *Wea. Forecasting,* **21,** 735–751.

Garner, J. M., 2012: Environments of significant tornadoes occurring within the warm sector versus those occurring along surface baroclinic boundaries. *Electron. J. Severe Storms Meteor.,* **7** (5). [Available online at http://www.ejssm.org/ojs/index.php/ejssm/article/viewArticle/101.]

Gensini, V. A., and W. S. Ashley, 2011: Climatology of potentially severe convective environments from the North American Regional Reanalysis. *Electron. J. Severe Storms Meteor.,* **6** (8). [Available online at http://www.ejssm.org/ojs/index.php/ejssm/article/viewArticle/85.]

Glass, F. H., D. L. Ferry, J. T. Moore, and S. M. Nolan, 1995: Characteristics of heavy rainfall events across the mid-Mississippi valley during the warm season: Meteorological conditions and conceptual model. Preprints, *14th Conf. on Weather Analysis and Forecasting,* Dallas, TX, Amer. Meteor. Soc., 34–41.

Grams, J. S., R. L. Thompson, D. V. Snively, J. A. Prentice, G. M. Hodges, and L. J. Reames, 2012: A climatology and comparison of parameters for significant tornado events in the United States. *Wea. Forecasting,* **27,** 106–123.

Hagemeyer, B. C., 1997: Peninsular Florida tornado outbreaks. *Wea. Forecasting,* **12,** 399–427.

Hales, J. E., 1988: Improving the watch/warning system through the use of significant event data. Preprints, *15th Conf. Severe Local Storms,* Baltimore, MD, Amer. Meteor. Soc., 165–168.

Hart, J., and J. Korotky, 1991: The SHARP workstation v1.50: A Skew-T/hodograph analysis and research program for the IBM and compatible PC—User's manual. National Weather Service, 62 pp.

Holton, J. R., 1967: The diurnal boundary-layer wind oscillation about sloping terrain. *Tellus,* **19,** 199–205.

Johns, R. H., 1984: A synoptic climatology of northwest-flow severe weather outbreaks. Part II: Meteorological parameters and synoptic patterns. *Mon. Wea. Rev.,* **112,** 449–464.

——, and C. A. Doswell III, 1992: Severe local storms forecasting. *Wea. Forecasting,* **7,** 558–612.

Koch, S. E., D. Hamilton, D. Kramer, and A. Langmaid, 1998: Mesoscale dynamics in the Palm Sunday tornado outbreak. *Mon. Wea. Rev.,* **126,** 2031–2060.

Lowe, A. B., and G. A. McKay, 1962: Tornado composite charts for the Canadian prairies. *J. Appl. Meteor.,* **1,** 157–162.

Maddox, R. A., and C. A. Doswell III, 1982: An examination of jet stream configurations, 500 mb vorticity advection and low-level

thermal advection patterns during extended periods of intense convection. *Mon. Wea. Rev.,* **110,** 184–197.

——, L. R. Hoxit, and C. F. Chappell, 1980: A study of tornadic thunderstorm interactions with thermal boundaries. *Mon. Wea. Rev.,* **108,** 322–336.

Markowski, P. M., E. N. Rasmussen, and J. M. Straka, 1998: The occurrence of tornadoes in supercells interacting with boundaries during VORTEX-95. *Wea. Forecasting,* **13,** 852–859.

——, C. Hannon, J. Frame, E. Lancaster, A. Pietrycha, R. Edwards, and R. L. Thompson, 2003: Characteristics of vertical wind profiles near supercells obtained from the Rapid Update Cycle. *Wea. Forecasting,* **18,** 1262–1272.

McNulty, R. P., 1978: On upper tropospheric kinematics and severe weather occurrence. *Mon. Wea. Rev.,* **106,** 662–672.

Mead, C. M., and R. L. Thompson, 2011: Environmental characteristics associated with nocturnal significant-tornado events in the central and southern Great Plains. *Electron. J. Severe Storms Meteor.,* **6** (6). [Available online at http://www.ejssm.org/ojs/index.php/ejssm/article/viewArticle/84.]

Messinger, F., and Coauthors, 2006: North American Regional Reanalysis. *Bull. Amer. Meteor. Soc.,* **87,** 343–360.

Miller, R. C., 1972: Notes on analysis and severe storms forecasting procedures of the Air Force Global Weather Central. Air Weather Service Tech. Rep. 200 (rev.), 181 pp.

Monteverdi, J. P., C. A. Doswell III, and G. S. Lipari, 2003: Shear parameter thresholds for forecasting tornadic thunderstorms in northern and central California. *Wea. Forecasting,* **18,** 357–370.

Mook, C. P., 1954: A preferred thickness line accompanying multiple tornado occurrences. *Mon. Wea. Rev.,* **82,** 160–162.

Moore, J. T., F. H. Glass, C. E. Graves, S. M. Rochette, and M. J. Singer, 2003: The environment of warm-season elevated thunderstorms associated with heavy rainfall over the central United States. *Wea. Forecasting,* **18,** 861–878.

Purdom, J. F. W., 1976: Some uses of high-resolution GOES imagery in the mesoscale forecasting of convection and its behavior. *Mon. Wea. Rev.,* **104,** 1474–1483.

Rasmussen, E. N., and R. B. Wilhelmson, 1983: Relationships between storm characteristics and 1200 GMT hodographs, low-level shear, and stability. Preprints, *13th Conf. on Severe Local Storms,* Tulsa, OK, Amer. Meteor. Soc., J5–J8.

——, and D. O. Blanchard, 1998: A baseline climatology of sounding-derived supercell and tornado forecast parameters. *Wea. Forecasting,* **13,** 1148–1164.

——, J. M. Straka, R. P. Davies-Jones, C. A. Doswell III, F. H. Carr, M. D. Eilts, and D. R. MacGorman, 1994: The Verification of the Origins of Rotation in Tornadoes Experiment: VORTEX. *Bull. Amer. Meteor. Soc.,* **75,** 997–1006.

——, S. Richardson, J. M. Straka, P. M. Markowski, and D. O. Blanchard, 2000: The association of significant tornadoes with a baroclinic boundary on 2 June 1995. *Mon. Wea. Rev.,* **128,** 174–191.

Rose, S. F., P. V. Hobbs, J. D. Locatelli, and M. T. Stoelinga, 2004: A 10-yr climatology relating the locations of reported tornadoes to the quadrants of upper-level jet streaks. *Wea. Forecasting,* **19,** 301–309.

Schumacher, P. N., and J. M. Boustead, 2011: Mesocyclone evolution associated with varying shear during the 24 June 2003 tornado outbreak. *Wea. Forecasting,* **26,** 808–827.

Thompson, R. L., 1998: Eta Model storm-relative winds associated with tornadic and nontornadic supercells. *Wea. Forecasting,* **13,** 125–137.

——, and R. Edwards, 2000: An overview of environmental conditions and forecast implications of the 3 May 1999 tornado outbreak. *Wea. Forecasting,* **15,** 682–699.

——, ——, J. A. Hart, K. L. Elmore, and P. Markowski, 2003: Close proximity soundings within supercell environments obtained from the Rapid Update Cycle. *Wea. Forecasting,* **18,** 1243–1261.

——, B. T. Smith, J. S. Grams, and A. R. Dean, 2012: Convective model for significant severe thunderstorms in the contiguous United States. Part II: Supercell and QLCS tornado environments. *Wea. Forecasting,* **27,** 1136–1154.

Uccellini, L. W., and D. R. Johnson, 1979: The coupling of upper and lower tropospheric jet streaks and implications for the development of severe convective storms. *Mon. Wea. Rev.,* **107,** 682–703.

Weaver, J. F., and J. F. W. Purdom, 1995: An interesting mesoscale storm–environment interaction observed just prior to changes in severe storm behavior. *Wea. Forecasting,* **10,** 449–453.

Weisman, M. L., C. Davis, W. Wang, K. W. Manning, and J. B. Klemp, 2008: Experiences with 0–36-h explicit convective forecasts with the WRF-ARW model. *Wea. Forecasting,* **23,** 407–437.

Whiting, R. M., and R. E. Bailey, 1957: Some meteorological relationships in the prediction of tornadoes. *Mon. Wea. Rev.,* **85,** 141–150.

Wilks, D. S., 1995: *Statistical Methods in the Atmospheric Sciences: An Introduction.* Academic Press, 467 pp.